Arabidopsis KCBP interacts with AIR9 but stays in the cortical division zone throughout mitosis via its MyTH4-FERM domain

Buschmann H., Dols J., Kopischke S., Pena E.J., Andrade-Navarro M.A., Heinlein M., Szymanski D.B., Zachgo S., Doonan J.H., Lloyd C.W.

Journal of Cell Science
2015 JUN 01 ; 28(11): 2033-2046
doi: 10.1242/jcs.156570
Publisher: The Company of Biologists Ltd

© 2015. Published by The Company of Biologists Ltd | Journal of Cell Science (2015) 128, 2033-2046 doi:10.1242/jcs.156570

RESEARCH ARTICLE

Arabidopsis KCBP interacts with AIR9 but stays in the cortical division zone throughout mitosis via its MyTH4-FERM domain

Henrik Buschmann[1,*,‡‡], Jacqueline Dols[1,‡], Sarah Kopischke[2], Eduardo J. Peña[3,§], Miguel A. Andrade-Navarro[4,], Manfred Heinlein[3], Daniel B. Szymanski[5], Sabine Zachgo[2], John H. Doonan[1,¶] and Clive W. Lloyd[1]**

ABSTRACT

The preprophase band of microtubules performs the crucial function of marking the plane of cell division. Although the preprophase band depolymerises at the onset of mitosis, the division plane is 'memorized' by a cortical division zone to which the phragmoplast is attracted during cytokinesis. Proteins have been discovered that are part of the molecular memory but little is known about how they contribute to phragmoplast guidance. Previously, we found that the microtubule-associated protein AIR9 is found in the cortical division zone at preprophase and returns during cell plate insertion but is absent from the cortex during the intervening mitosis. To identify new components of the preprophase memory, we searched for proteins that interact with AIR9. We detected the kinesin-like calmodulin-binding protein, KCBP, which can be visualized at the predicted cortical site throughout division. A truncation study of KCBP indicates that its MyTH4-FERM domain is required for linking the motor domain to the cortex. These results suggest a mechanism by which minus-end-directed KCBP helps guide the centrifugally expanding phragmoplast to the cortical division site.

KEY WORDS: AIR9, Kinesin, Cell division, MyTH4-FERM, Preprophase band, *Arabidopsis*

INTRODUCTION

The preprophase band (PPB) of microtubules was first observed in electron microscopic studies on higher plant cell division performed in the 1960s (Pickett-Heaps and Northcote, 1966). This premitotic ring was seen to predict the edge of the plane where, after nuclear division, the outwardly growing cell plate would make contact with the mother cell wall (Jürgens, 2005; Müller, 2012). Although a few specialized types of higher plant cells were later found to divide without first forming a preprophase band, the presence of this structure in most cells was found to accurately predict all varieties of division plane: curved or straight, periclinal or anticlinal, and symmetric or asymmetric. In these cases, the preprophase band always disappeared before the cytokinetic apparatus could construct the dividing wall in the predicted plane. This gave rise to the idea that the disappearing preprophase band imprinted some kind of 'memory' at the cortical division site, acting as a molecular beacon to guide the edge of the phragmoplast to the predicted cortical zone (Gunning and Wick, 1985; Mineyuki, 1999; Van Damme et al., 2007).

Best seen in large vacuolated cells, the division plane is also memorized by the cytoplasm that forms a transvacuolar division disc (the phragmosome), which suspends the chromatin throughout mitosis and cytokinesis. Actin filaments pervade the phragmosome and continue into the preprophase band that marks the perimeter of the disc (Traas et al., 1987). However, by metaphase, actin filaments depolymerize in a narrow ring within the wider ring that was once marked by the preprophase band. This constitutes the actin-depleted zone, which represents a negative marker of the future phragmoplast attachment site (Cleary, 1995). Actin is not, however, completely absent from the vicinity of the wider cortical division zone (CDZ) because F-actin is enriched at either side of the actin-depleted zone to form what has been termed 'actin twin peaks' (Sano et al., 2005). Another negative marker of the CDZ is the KCA1 kinesin (Vanstraelen et al., 2006). Like actin, it is found at the plasma membrane of dividing cells but is excluded from the CDZ itself.

The first marker reported to remain at the division site from preprophase to cytokinesis was the plant-specific protein TANGLED (TAN) (Walker et al., 2007). The GTPase-activating protein of the small GTPase Ran (RanGAP1) was also found to remain at the CDZ throughout division (Xu et al., 2008). The recruitment of RanGAP1 to the preprophase band requires FASS/TONNEAU2 (Torres-Ruiz and Jürgens, 1994; Camilleri et al., 2002; Spinner et al., 2013), an upstream regulatory subunit of protein phosphatase 2A found to be essential for preprophase band assembly. Persistence of RanGAP1 at the cortical division site beyond preprophase, however, is dependent on two kinesins, POK1 and POK2 (Müller et al., 2006) – kinesins that are implicated in the association of TAN with the predicted division site. A recent publication shows that the POK1 kinesin too is a continuous marker of the cell division plane and remains attached to the cortex from prophase to cytokinesis (Lipka et al., 2014). FASS/TONNEAU2 itself, or at least its maize homologue DISCORDIA1, remains in the CDZ until metaphase, after which it disappears from the cortex (Wright et al., 2009).

Another class of markers has emerged that does positively mark the CDZ but only fleetingly given that they disappear along with the preprophase band microtubules by metaphase. Such evanescent markers are unlikely therefore to 'memorize' the division site until

[1]Department of Cell and Developmental Biology, John Innes Centre, Norwich, Norfolk NR4 7UH, UK. [2]Botanical Institute, Biology and Chemistry Department, University of Osnabrück, 49069 Osnabrück, Germany. [3]Institut de Biologie Moléculaire des Plantes, UPR2357 CNRS, Strasbourg, France. [4]Max Delbrück Center for Molecular Medicine, 13125 Berlin, Germany. [5]Department of Agronomy, Purdue University, West Lafayette, IN 47907, USA.
*Present address: Botanical Institute, Biology and Chemistry Department, University of Osnabrück, 49076 Osnabrück, Germany. ‡Present address: Max Planck Institute for Biology of Ageing, Department for Biological Mechanisms of Ageing, 50931 Cologne, Germany. §Present address: Instituto de Biotecnología y Biología Molecular, CCT – La Plata CONICET, Fac. Cs. Exactas, U.N.L.P., 1900 La Plata, Argentina. ¶Present address: National Plant Phenomics Centre, IBERS, Aberystwyth University, Aberystwyth SY23 3EB, UK. **Present address: Johannes Gutenberg University of Mainz and Institute of Molecular Biology, Ackermannweg 4, 55128 Mainz, Germany.

‡‡Author for correspondence (Henrik.Buschmann@biologie.uni-osnabrueck.de)

Received 28 May 2014; Accepted 10 April 2015

Journal of Cell Science

Journal of Cell Science (2015) 128, 2033-2046 doi:10.1242/jcs.156570

cytokinesis; these include several kinesin-like proteins, cell cycle regulators and mitogen-activated protein kinases (MAPKs) (Van Damme et al., 2007; Rasmussen et al., 2011a; Lipka and Müller, 2012). The CDZ is also a region specialized for membrane transport. A so-called 'Golgi belt' – an accumulation of Golgi stacks present in the cytoplasm underlying the division zone – was seen during the mitosis of dividing tobacco BY-2 cells (Nebenführ et al., 2000). Although the presence of the Golgi belt could indicate that division plane alignment requires exocytosis, transient application of the exocytosis inhibitor brefeldin A at prophase suggested that Golgi secretion is not required for marking the cortical division site (Dixit and Cyr, 2002). However, there is now good evidence that clathrin-mediated endocytosis is enhanced in the region of the CDZ at prophase (Karahara et al., 2009). Furthermore, the *Arabidopsis* TPLATE protein, which shows similarity to adaptin and coatomer proteins and which physically interacts with *Arabidopsis* clathrin light chain 2, localized to cell plates and, during cytokinesis, specifically to the CDZ. However, TPLATE is excluded from the narrower ring where the cell plate will insert. Knockdown of TPLATE interferes with cell plate insertion and it appears that membrane traffic involving TPLATE is required to complete cytokinesis (Van Damme et al., 2006; Van Damme et al., 2011).

All of this indicates that some proteins mark (positively or negatively) a wider division belt around the cell, whereas others define a more restricted – but more accurately predictive – ring. This distinction has been emphasized by Van Damme et al. (Van Damme et al., 2011) who proposed that the term CDZ be reserved for the wider cortical band while the narrow ring it brackets be known as the cortical division site. This appreciation of two functionally different molecular zones agrees with observations that the preprophase band of microtubules becomes narrower upon the cortex before it disappears (Mineyuki et al., 1989) and also with the fact that the preprophase memory sharpens as the cell progresses from metaphase to cytokinesis, as in the case of TAN (Walker et al., 2007; Rasmussen et al., 2011b). Furthermore, TAN contains two functional domains: one that targets TAN to the CDZ in preprophase and another that facilitates the return of TAN to the cortex at cytokinesis (Rasmussen et al., 2011b). This supports the idea that the CDZ functionally matures as it progresses from prophase to cytokinesis.

Our previous work has shown that a large microtubule-associated protein from *Arabidopsis,* AIR9 (auxin-induced in root cultures 9), seems to have a critical role in cytokinesis and cross-wall maturation (Buschmann et al., 2006; Buschmann et al., 2007). AIR9 colocalizes with the preprophase band but, unlike TAN and RanGAP1, is not present in the CDZ once the preprophase band has depolymerized. However, in contrast to the evanescent class of markers cited above, AIR9 does reappear at the cortex as a tight ring just as the expanding phragmoplast makes contact with the cortical division site. Once the phragmoplast contacts the former preprophase band site, AIR9 invades the nascent cell plate forming a torus. Drug-induced formation of supernumerary branches of the phragmoplast has shown that an AIR9 torus forms only where the cell plate becomes attached at the former preprophase band site, but not at any other cortical site unmarked by a preprophase band. This suggests that AIR9 specifically interacts with proteins constituting the preprophase memory. In addition, a truncation study of AIR9 confirmed that microtubule binding and preprophase band memory interaction are represented by separate regions within the AIR9 protein: the positively charged N-terminus and the large region containing the repeated A9 domains, respectively (Buschmann et al., 2006). Homologues of AIR9 are present in certain bacteria and protozoa (Buschmann et al., 2007). Interfering with the function of the AIR9 homologue from *Trypansoma brucei* results in defects in nuclear positioning and cleavage furrow placement (May et al., 2012).

To find out more about the functional composition of the molecular memory of the preprophase band, we exploited the ability of AIR9 to 'remember' the CDZ and searched for interaction partners that bind its region of repeated A9 domains. One such protein was KCBP, the kinesin-like calmodulin-binding protein, which features a C-terminal motor domain that moves along microtubules in the minus direction (Reddy et al., 1996; Oppenheimer et al., 1997; Song et al., 1997). We find that KCBP, when expressed from the endogenous promoter, labels the cortical division site throughout mitosis. KCBP also contains an N-terminal myosin tail homology 4 and band4.1, ezrin, radixin, moesin (MyTH4-FERM) domain (Richardson et al., 2006). Using truncation studies, we show that loss of this domain abolishes the ability of KCBP to locate to the cortical division site. We consider mechanisms by which microtubule minus-end-directed motors like KCBP could guide the outgrowing phragmoplast to the cortical division site.

RESULTS

The dynamic behaviour of AIR9 during cell division

We previously determined the 187 kDa AIR9 protein from *Arabidopsis thaliana* (L.) Heynh., which is expressed in cycling cell suspension cultures, is a microtubule-associated protein (Buschmann et al., 2006). To establish that the *AIR9* gene is involved in cell division *in planta* we generated a fusion of the 1852 bp *AIR9* promoter with the *Escherichia coli* β-glucuronidase (GUS) coding sequence. In transgenic *Arabidopsis*, the AIR9 promoter directed the expression of GUS to root meristems. GUS expression was also seen in the root stele (Fig. 1A). In aerial parts of the plants, the *AIR9* promoter was active in young leaves, in trichomes of young and of mature leaves, and in the vasculature of leaves and stems (supplementary material Fig. S1). To verify that *AIR9* is expressed in dividing cells we performed whole-mount *in situ* mRNA hybridization of *Arabidopsis* roots using an *AIR9* antisense probe. The probe stained the meristematic region of the root tip, supporting the conclusion that AIR9 is expressed strongest in dividing cells (Fig. 1B,C).

GFP–AIR9 expression in cycling tobacco BY-2 cells, driven by the CaMV35S promoter, labels the preprophase band and, during the late phragmoplast stage, the cortical division site. GFP–AIR9 subsequently moves into the new cross wall forming a torus (Buschmann et al., 2006). To analyse cell division in *Arabidopsis* root tips, the same construct was transformed into wild-type Col-0 plants. Spinning disc confocal microscopy confirmed that the localization of the GFP–AIR9 fusion in root meristems followed the same pattern previously reported in tobacco BY-2 cells (supplementary material Fig. S2). However, because of the stronger signal in BY-2 suspension cells, this tobacco cell line was used as the model for the high-resolution analysis of AIR9 behaviour during cell division (Fig. 1D–F; supplementary material Movie 1). Double labelling of tobacco BY-2 cell division with GFP–tubulin showed that mRFP1–AIR9 does not bind to spindle microtubules (Fig. 1G–I). After cytokinesis, GFP–AIR9 tends to label the new cross wall (Buschmann et al., 2006), which was also clearly seen in root tips of transgenic 35S::GFP–AIR9 plants (Fig. 1J). To investigate whether the strong cross-wall label is independent of microtubules, we investigated the effect of microtubule-depolymerizing oryzalin using tobacco BY-2 cells. In this case, GFP–AIR9 was still found on the

Journal of Cell Science (2015) 128, 2033-2046 doi:10.1242/jcs.156570

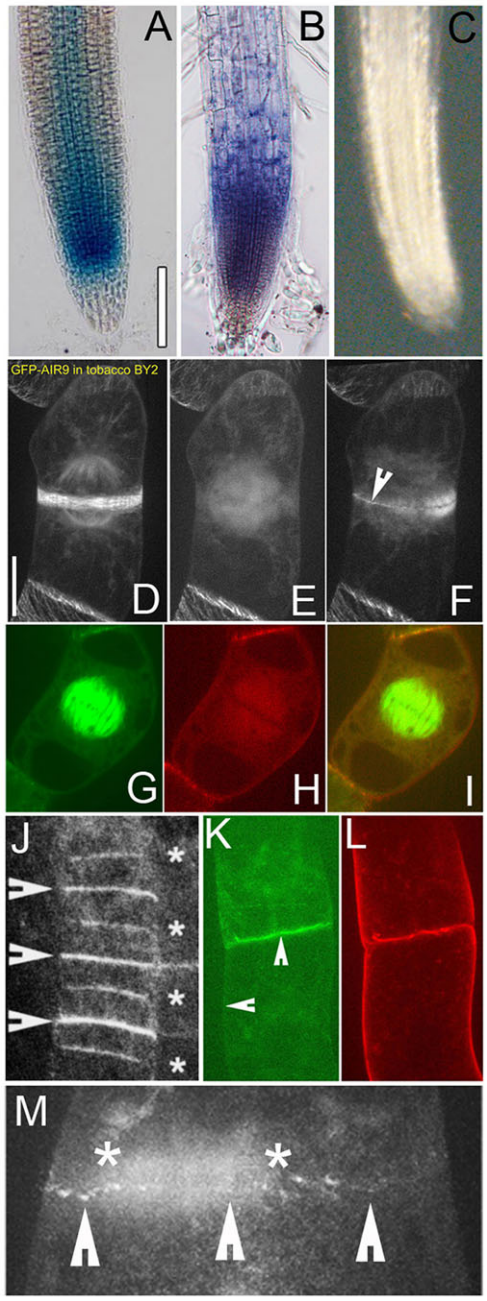

Fig. 1. AIR9 is expressed in dividing cells and interacts with the cortical division site. (A) β-glucuronidase expression directed by the *Arabidopsis AIR9* promoter to the root tip meristem and to the vasculature. (B) An *AIR9* antisense probe was used in whole-mount RNA *in situ* localization and revealed expression in the meristem. (C) Negative control for *in situ* hybridization experiment. (D–F) In tobacco BY-2 cells, GFP-labelled AIR9 labelled the cortical division site at preprophase and during cytokinesis (arrowhead). (E) During metaphase, microtubule labelling was apparently downregulated. (G–I) In double labelling experiments in tobacco BY-2 cells for GFP-tubulin (G) and mRFP1–AIR9 (H), diffuse labelling of the metaphase spindle by AIR9 was seen, but merging the channels (I) suggested low affinity of mRFP1–AIR9 for microtubules at this stage. (J) In *Arabidopsis* root meristems GFP–AIR9 had a strong affinity for crosswalls. The alternating patterns suggested that new (arrowheads) and old (asterisks) cross walls were occupied to varying extents. (K–L) In tobacco BY-2 cells, GFP–AIR9 labelled the plasma membrane of cross walls and this was independent of microtubules. (K) When microtubules were depolymerized using oryzalin, GFP–AIR9 remained present on cross walls, but not on sidewalls (compare horizontal and vertical arrowheads). (L) Same cell as in K stained with the membrane dye FM4-64. (M) The ability of GFP–AIR9 to recognize the cortical division site of tobacco BY-2 cells was demonstrated using the inhibitor brefeldin A. When brefeldin A was applied during mitosis, GFP–AIR9 was seen to label the cortical division site prematurely (early telophase). In such experiments the phragmoplast was often seen to collapse before reaching the cortex (arrowheads in M; asterisks indicate approximate position of the phragmoplast). Scale bars: 200 µm (A); 20 µm in (D–I,K,L).

cross wall, indicating that AIR9 binds some other component of the cortex in the absence of microtubules (Fig. 1K,L).

We previously reported that GFP–AIR9 disappears from the CDZ after preprophase but returns to the cortex just as the cell plate inserts (Buschmann et al., 2006). To clarify whether GFP–AIR9 arrives at this location through the approaching microtubules of the phragmoplast, or whether its localization is independent of the phragmoplast, we applied brefeldin A, because this drug has been shown in BY-2 cells to cause the phragmoplast to stop growing and collapse after prolonged incubation (Reichardt et al., 2007). Interestingly, when brefeldin A was applied during the spindle stage, GFP–AIR9 could be seen to label the cortical division site prematurely during the early phragmoplast stage (arrows point at the dotted cortical AIR9 signal) rather than at the stage of cell plate attachment (Fig. 1M). This demonstrates that cortical GFP–AIR9 is capable of binding the cortical division site independently of the approaching phragmoplast (framed by asterisks). This also emphasizes that AIR9 is capable of recognizing and binding a component of the cortical division site but that this ability is normally suppressed during the spindle and early phragmoplast stages of division (Fig. 1M).

AIR9 physically interacts with KCBP

Based on our previous study and the results presented in Fig. 1, we hypothesized that AIR9 physically interacts with a component of the preprophase memory. To identify this component we initiated a yeast two-hybrid (Y2H) screen. Because the truncation study of AIR9 (Buschmann et al., 2006) had raised the possibility that the 11 repeated A9 domains of AIR9 might be sufficient for interacting with the preprophase memory, this large region (positions 455–1595, i.e. 1141 amino acids) was subcloned and used in a Y2H screen against an *Arabidopsis* seedling library. Several putative protein interactors were identified but the calmodulin-regulated kinesin KCBP represented the best 'hit'. We obtained 12 N-terminal fragments of KCBP that, based on sequencing, were likely to be independent clones. Sequence alignment with full-length KCBP allowed us to determine the minimal KCBP sequence required for interacting with AIR9. The minimal KCBP sequence encompassed a part of the FERM domain (i.e. the FERM-M and FERM-C subdomains) including a part of the adjacent coiled coil region (Fig. 2A).

To verify the Y2H result, the interaction of AIR9 with KCBP was studied by immunoprecipitation. This was done using a rabbit antibody against AIR9 (Basu et al., 2005) and a rat antibody against cotton KCBP (Preuss et al., 2003). Initial experiments showed that the antibody against cotton KCBP cross-reacted with *Arabidopsis* KCBP from cycling *Arabidopsis* cell suspensions [a green cell line of Landsberg *erecta* (L*er*) ecotype]. The same suspension cell line was used in subsequent tests because AIR9 was highly expressed in these cycling cells. For pulldown experiments, cell extracts from the L*er* line were exposed to the AIR9 antibody (see Materials and Methods). After pulldown with protein A beads and analysis by SDS-PAGE, a single band of 140 kDa could be detected in western blots (Fig. 2B), indicating that AIR9 interacts with KCBP in cycling cells in suspension.

Journal of Cell Science (2015) 128, 2033-2046 doi:10.1242/jcs.156570

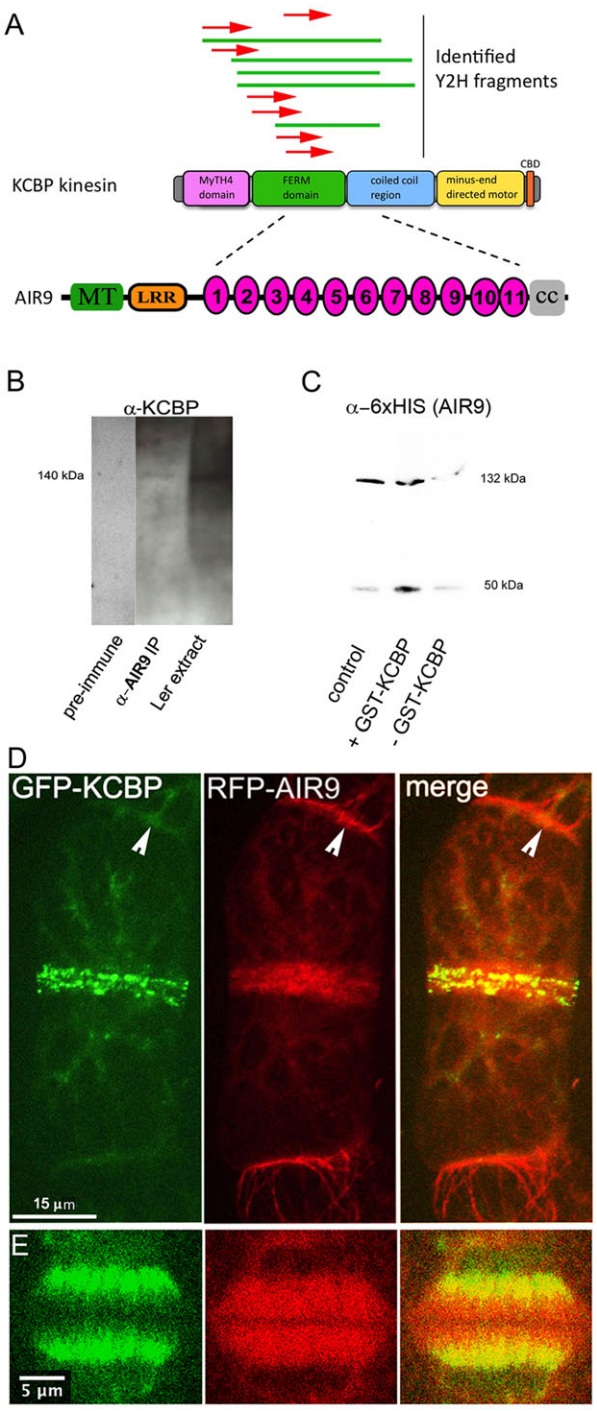

Fig. 2. AIR9 interacts with the minus-end-directed kinesin KCBP. (A) A yeast two-hybrid screen was initiated using the eleven repeated A9 domains present in AIR9. In this screen, the kinesin KCBP was recovered with several independent fragments. Green bars indicate fragments for which the 5′ and 3′ ends were determined by sequencing. Red arrows indicate fragments for which only the 5′ sequence is known. The dashed lines indicate the AIR9 fragment used in the yeast experiment and the minimal region in KCBP needed for the interaction. Accordingly, the C-terminal half of the FERM domain in KCBP and part of the adjacent coiled coil region was sufficient for AIR9 interaction. (B) Immunoprecipitation experiments based on plant extracts showed that AIR9 binds to KCBP. AIR9 from *Arabidopsis* L*er* suspension cells was pulled down using the anti-AIR9 antibody. The immunoprecipitated proteins were then separated by electrophoresis, blotted and probed with the antibody against cotton KCBP. (C) Independent support for the interaction of AIR9 with KCBP using bacterially expressed proteins. His-tagged AIR9 was purified as two fragments, the complete 132 kDa fragment (including the eleven A9 repeated domains) and a smaller, ~50 kDa-sized fragment. Lane 1, purified HIS–AIR9 protein only; lane 2, HIS–AIR9 bound to GST–agarose beads in the presence of GST–KCBP; lane 3, in the absence of GST–KCBP. (D) A full-length cDNA of KCBP was cloned, coupled to GFP and co-expressed with mRFP1–AIR9 in tobacco BY-2 cells. Both genes were expressed using the CaMV35S promoter. Colocalization (yellow signal) was observed in the preprophase band of microtubules. Arrowheads show colocalization on cross walls. (E) KCBP (on left) and AIR9 (middle) further colocalize on phragmoplast microtubules (merge on right). Scale bars: 15 µm (D); 5 µm (E).

Next, we asked whether an interaction of AIR9 with KCBP could be observed using purified proteins. For this, full-length GST–KCBP was produced in *E. coli*. AIR9 was produced as an 1194-amino-acid fragment (amino acids 421–1614) tagged with N-terminal His_6, also in *E. coli* (total 132 kDa). This fragment of AIR9 contains the entire region of the A9 repeated domains (similar to that used in the Y2H experiment). Nickel-column purification of His–AIR9, however, produced two bands – a larger band corresponding to the 132 kDa fragment and a smaller ~50 kDa band that was also detected by the anti-His antibody and was presumed to be an N-terminal truncation product. The purified, desalted and concentrated KCBP and AIR9 proteins were mixed and incubated with agitation at room temperature. Next, equilibrated glutathione–agarose beads were added and the mixture was further incubated. The beads were then centrifuged, washed, boiled in SDS-buffer and subjected to western blot analysis. Binding in the presence of GST–KCBP was greatly enhanced above the background binding of His–AIR9 to the beads (Fig. 2C). This substantiates that there is a physical interaction between KCBP and AIR9, and suggests the interaction is direct. Interestingly, the smaller ~50 kDa N-terminal truncation product of the His–AIR9 fragment also interacted with GST–KCBP, suggesting that a KCBP interaction domain resides in this region.

Next, we investigated whether AIR9 and KCBP colocalize during cell division. For initial experiments, a cDNA of KCBP was cloned and tagged with C-terminal or N-terminal GFP. These fusions were expressed in cycling tobacco BY-2 cells using the CaMV35S promoter. We found that both fusions of KCBP localized to the preprophase band in a punctate manner. The tagged KCBP constructs were then co-transformed with mRFP1–AIR9. mRFP1–AIR9 and GFP-tagged KCBP colocalized in the preprophase band of tobacco BY-2 cells (Fig. 2D). Colocalization was also observed on the cross-walls (arrowheads in Fig. 2D) and on the distal half of phragmoplast microtubules (Fig. 2E).

AIR9 recruits KCBP to interphase microtubules in *Nicotiana benthamiana*

To gain further insight into the interaction of AIR9 with KCBP, fusions of these proteins to fluorescent proteins were expressed in *Nicotiana benthamiana* (Domin) leaf epidermal cells using *Agrobacterium*-mediated transient transformation. When GFP–KCBP was expressed alone no, or only a few, microtubules were seen in these non-dividing cells. Instead, most of the label appeared to be cytoplasmic or weakly associated with a reticulate cytoplasmic system (Fig. 3A). When mRFP1–AIR9 was transformed alone, cortical microtubules became visible. mRFP1–AIR9 expression in the leaf cells caused microtubule bundling (Fig. 3B) that was also seen in other experiments involving transient expression of AIR9 (e.g. in *Arabidopsis* suspension cells; supplementary material Fig. S3A). Surprisingly, co-expression of GFP–KCBP with mRFP1–AIR9 in leaf epidermal cells led to a dramatic shift in the

Journal of Cell Science (2015) 128, 2033-2046 doi:10.1242/jcs.156570

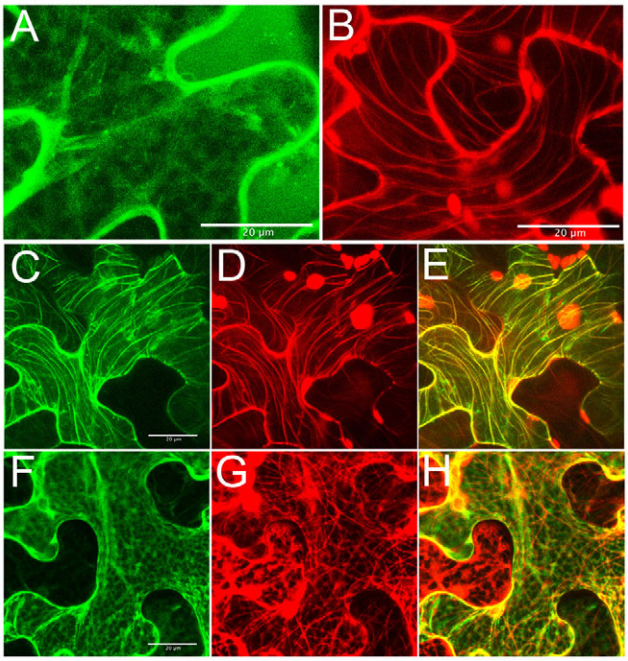

Fig. 3. The localization of GFP–KCBP in *N. benthamiana* interphase cells depends on AIR9 co-expression. (A) When GFP–KCBP was expressed in the absence of mRFP1–AIR9, it labelled the cytoplasm (as seen in cytoplasmic strands) and a somewhat reticulate structure at the cortex of the cell. (B) Expression of the MAP, mRFP1–AIR9, led to microtubule bundling. (C–E) When GFP–KCBP (C) and mRFP1–AIR9 (D) were expressed in the same cell, KCBP became re-localized to AIR9-bundled microtubules. (E) Colocalization is demonstrated by merging the channels. (F–H) This was not seen when GFP–KCBP was co-expressed with the microtubule-binding domain of MAP4 (G). (H) Merged image. Scale bars: 20 µm.

localization of KCBP. In this case, GFP–KCBP could be seen to localize to microtubule bundles that were also labelled by mRFP1–AIR9. Merging of the channels showed extensive colocalization (Fig. 3C–E). This indicates that in epidermal leaf cells of *Nicotiana*, AIR9 is capable of recruiting KCBP to cortical microtubules. Similar results were obtained using the C-terminal GFP fusion of KCBP (supplementary material Fig. S3). As a control, we investigated the co-expression of GFP–KCBP with another microtubule-associated protein (MAP): the mRFP1-tagged microtubule-binding domain of mammalian MAP4. In to mRFP1–AIR9, mRFP1–MAP4 was not capable of recruiting KCBP to cortical microtubules (Fig. 3; supplementary material Fig. S3).

The phenotype of *air9* and *zwi* mutants

To deepen our understanding of *AIR9* and *ZWICHEL* gene function in cell division, we analysed respective mutants and double mutants. Screens for transposon mutants impaired in gametophytic development have repeatedly identified insertions into the *AIR9* single copy gene. We analysed in detail the transposon-induced *ungud9* (*air9-9*) mutant of *AIR9* (Lalanne et al., 2004) (Fig. 4A; supplementary material Table S1) and observed a dramatic reduction of pollen germination for *ungud9 in vitro* (data not shown). The defects in female gametophytic development included aberrations in cell division and ovule differentiation (Fig. 4B; for details see supplementary material Fig. S4A,B). However, when the hitherto unknown 5′ transposon border of *ungud9* was isolated it was found that the *ungud9* insertion is associated with a deletion of (at least) 11 genes starting from *AIR9*. By testing polymorphic markers we confirmed the presence of a large deletion using F1 plants of a cross between *ungud9* (L*er* ecotype) and Col-0 (Fig. 4A). Another transposon-induced mutant, *haumea*, shows a similar but even larger deletion (approximately 83 kb) that also includes part of the *AIR9* gene. *haumea* too has male and female transmission defects (Page et al., 2004). A third transposon-induced deletion mutant termed GT3730 shows a 5′ deletion of *AIR9* sequences but does not affect further genes. The reason for the high frequency of AIR9-associated deletions in transposon lines has to do with the fact that the T-DNA of the transposon starter line DSG-1 resides in *AIR9* (Sundaresan et al., 1995; Brodersen et al., 2002). Mechanisms for how this might result in large genomic deletions have been suggested to involve deletion of the negative selection marker *Indole Acetic Acid Hydrolase* from the DSG-1 T-DNA after inducing transposition (Page et al., 2004). Whereas *ungud9* and *haumea* have obvious defects in gametophytic development, no morphological phenotypes could be observed in the homozygous DSG-1 starter line (e.g. Fig. 4B) nor in the homozygous GT3730 line (data not shown).

In search for true *air9* phenotypes, additional T-DNA insertion lines were obtained from stock centres (supplementary material Table S1). Homozygous T-DNA insertions into *AIR9* showed severe disruption of *AIR9* transcription (Fig. 4C); however, no morphological phenotypes have so far been detected. The mutant *air9-5*, for example, shows apparently normal ovule development (Fig. 4B). When we quantified cell division plane alignment in roots, we found that the accuracy of cross wall placement in *air9-5* (also in *air9-27*) was highly similar, if not identical, to that in wild-type. Because AIR9 interacts with KCBP we were curious to analyse cell division plane alignment in the *zwichel* (*zwi*) mutants of KCBP. Such *zwi* mutants are best known for a defect in leaf trichome branching and expansion (Hülskamp et al., 1994; Oppenheimer et al., 1997). We quantified cross wall placement in the rhizodermis of *zwiA* (*zwiA* is a T-DNA insertion mutant of the SALK collection with a strong trichome phenotype; see Materials and Methods). No significant difference of cross wall placement in *zwiA* with respect to the wild-type could be detected (supplementary material Fig. S4C). We therefore created the double mutant of *air9-5* with *zwiA*. Again, in double homozygous *air9-5 zwiA* plants, division wall alignment was indistinguishable from wild-type (Fig. 4D; supplementary material Fig. S4C). Taken together, these results suggest that the function of *AIR9* and *ZWICHEL* in plant cell division might be redundant with additional genes. Uncovering these genes will help to establish a complete phenotypic description of *air9* and *zwi* mutations.

GFP–KCBP is a continuous resident of the CDZ in *Arabidopsis*

We next investigated whether GFP-tagged KCBP behaves similarly to GFP-tagged AIR9 during plant cell division. Previous localization studies of KCBP during cell division have necessarily used fixed material because they were based on immunofluorescence (Bowser and Reddy, 1997; Smirnova et al., 1998; Preuss et al., 2003). Therefore, to study KCBP localization in living cells the *Arabidopsis* KCBP promoter (Reddy and Reddy, 2004) was isolated and ligated into pGWB6, replacing the CaMV35S promoter. The resulting destination vector was recombined with an entry clone containing the entire *Arabidopsis* KCBP gene from its start codon, including all introns and its 3′ untranslated region. The genomic GFP-tagged KCBP construct was then used for complementation experiments using *zwiA* mutants. Transgenic *zwiA* plants carrying the genomic GFP–KCBP construct were identified by hygromycin and kanamycin selection on agar plates. Many, but not all, transgenic lines showed complementation of the *zwi* trichome phenotype (Fig. 5A,B). Complemented *zwiA* plants were investigated with

Journal of Cell Science (2015) 128, 2033-2046 doi:10.1242/jcs.156570

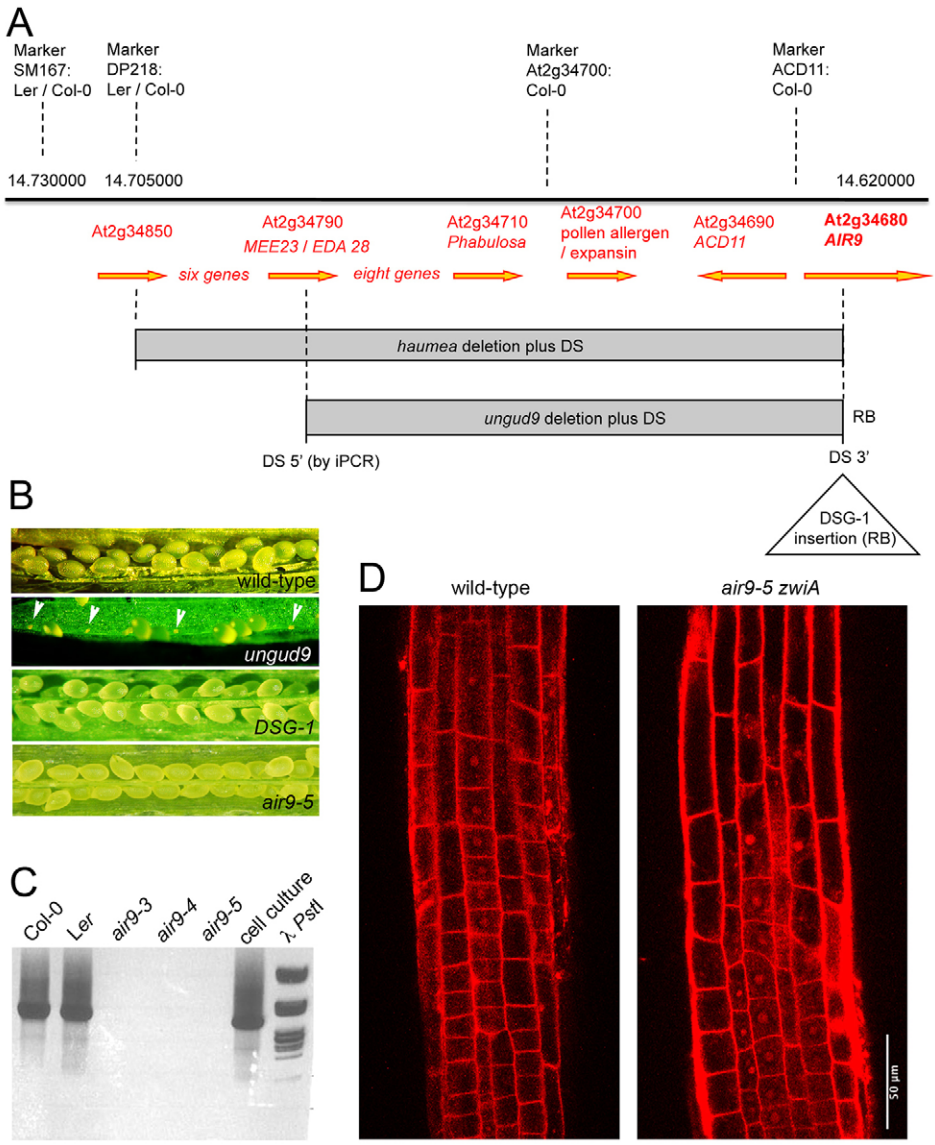

Fig. 4. Effects observed in mutants of the *Arabidopsis AIR9* gene. (A) The *ungud9* mutant of *AIR9* is characterized by a large deletion affecting at least 11 genes. Hemizygous *ungud9*/Col-0 plants were analysed by markers suitable for detecting Landsberg erecta/Col-0 polymorphisms. Results suggested the presence of a large deletion in *ungud9*. Next, the DS 5′ end of *ungud9* was isolated by inverse PCR and found to reside in At2g34790. Some genes possibly relevant to the *ungud9* gametophytic phenotype are indicated. The similar *haumea* mutant and the position of the DSG-1 T-DNA insertion are also indicated. (B) Siliques of wild-type, hemizygous *ungud9* and homozygous *air9-5* and DSG-1 plants. Note that only *ungud9* siliques present the failed ovule phenotype (arrowheads). (C) RT-PCR analysis of homozygous *AIR9* insertion mutants suggested severe disruption of *AIR9* gene transcription. The DNA marker is λ-*Pst*I. (D) Rhizodermal cell division patterns of wild-type and *air9-5 zwiA* double homozygous plants analysed by propidium iodide staining. Scale bar: 50 µm.

respect to GFP localization in the root. GFP signals were detectable but expression levels appeared to be low. Low magnification microscopy showed that GFP–KCBP expression was strongest in the root tip (Fig. 5C) although GFP–KCBP expression was still detectable in the elongation zone and in root hairs. Closer examination of the root tip showed that GFP–KCBP localizes to cross walls of interphase cells (Fig. 5D), similar to what was seen for GFP–AIR9 in meristems (Fig. 1). In dividing cells, GFP–KCBP localized to preprophase bands during premitosis then remained in the CDZ throughout mitosis and cytokinesis (Fig. 5E–G). GFP–KCBP was also seen towards the poles of the anaphase spindle (Fig. 5F) and on the phragmoplast (Fig. 5G) but was absent from the metaphase spindle.

Detailed analysis of GFP–KCBP localization in tobacco BY-2 cells

Because of the superior characteristics of tobacco BY-2 for the microscopy of cell division, we analysed the localization of GFP–KCBP in this cell line. CaMV35S-driven GFP–KCBP constructs in tobacco BY-2 cells underwent silencing quickly and it was hard to obtain data for the entire process of cell division (however, some movies were obtained by picking early colonies from transformation plates; see e.g. supplementary material Movie 2). By contrast, transformation with the genomic GFP–KCBP construct led to improved fluorescence and cell-cycle-dependent microtubule labelling in tobacco BY-2 cells (Fig. 6). GFP–KCBP expressed from its own promoter could be seen in the preprophase band, where it localized to foci arranged in a belt-like manner (Fig. 6A). At pro-metaphase, when the nuclear envelope disintegrated, GFP–KCBP remained at the cortex but did not label the spindle (Fig. 6B). During metaphase, the GFP–KCBP signal remained in the cortex, becoming slightly narrower. Metaphase spindles were not stained (Fig. 6C). At the anaphase–telophase transition (Fig. 6D), the cortical GFP–KCBP signal narrowed further and GFP–KCBP could then be seen at distal poles of the developing phragmoplast, where most microtubule minus-ends are found (Smertenko et al., 2011). From the phragmoplast stage onwards, the cortical GFP–KCBP signal was arranged like beads on a string (Fig. 6E,F). Throughout phragmoplast development, GFP–KCBP tended to accumulate towards the distal end of the phragmoplast rather than towards the proximal cell plate (see *z*-projection in Fig. 6F, and single section in Fig. 6G). GFP–KCBP was not found on the cell plate during the phragmoplast stage (Fig. 6G) but

Journal of Cell Science (2015) 128, 2033-2046 doi:10.1242/jcs.156570

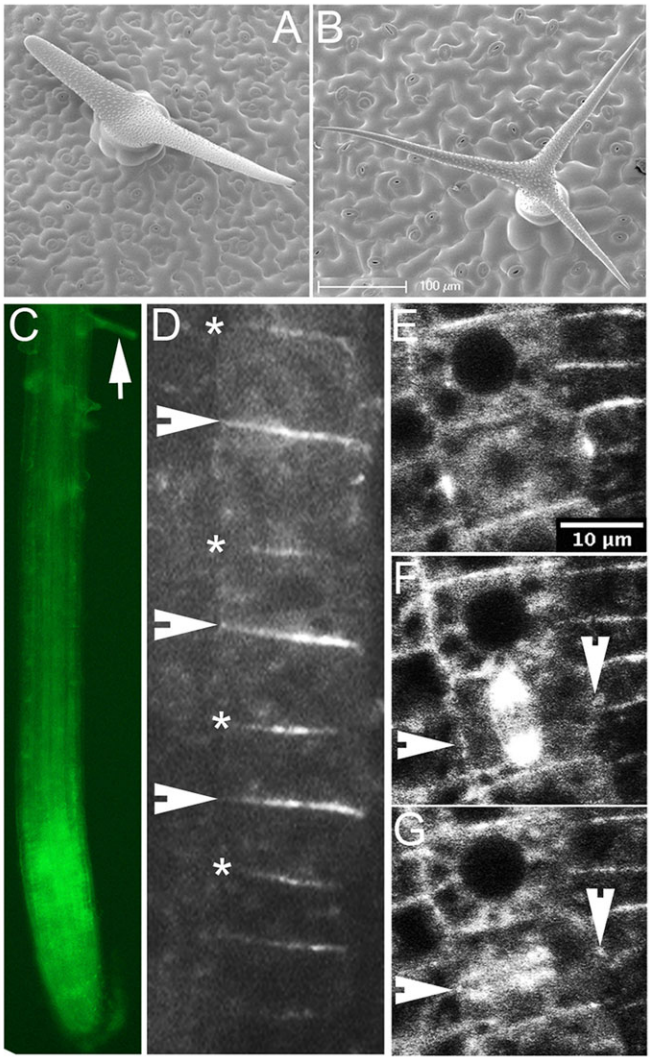

Fig. 5. The genomic GFP–KCBP fusion complements the *zwichel* mutant and confirms that KCBP localizes to the CDZ *in planta*. (A) The phenotype of a typical leaf trichome in the strong *zwiA* mutant. The *zwiA* mutation is in the Col-0 background. (B) Transformation of the genomic GFP–KCBP fusion complemented the trichome phenotype. (C) In the complemented plants, GFP expression of the root was strongest in the meristem and early elongation zone. However, GFP expression was often seen up to and including the root hairs (arrow). (D) A single confocal section approximately through the middle of a cell file revealed GFP–KCBP localization to cross walls of interphase cells. Labelling was stronger on alternating cross walls as denoted by arrowheads and asterisks. (E–G) During cell division GFP–KCBP localized to the CDZ. The cell division sequence is presented as single confocal planes. (E) As expected, KCBP localized to the preprophase band. Note that KCBP remained in the CDZ after preprophase band breakdown, and is visible in anaphase (F) and telophase (G) (arrowheads). Scale bars: 100 μm (A,B); 10 μm (E–G).

after cytokinesis some of the GFP–KCBP label moved into the new cross wall, forming a torus as previously described for AIR9 (arrowhead in Fig. 6H) (Buschmann et al., 2006).

Taken together, the results presented in Fig. 5, Fig. 6 and supplementary material Movie 2 indicate that KCBP is a continuous marker of the cortical division site in higher plants. The 1:1 colocalization of the KCBP signal with the lipid dye FM4-64 during metaphase (Fig. 6I) demonstrates the close association between the kinesin and the plasma membrane at a stage during which no cortical microtubules are present.

Colocalization of KCBP with microtubules during preprophase and cytokinesis

Next, we investigated the relationship between KCBP localization and microtubule positioning by double labelling. For this, we used transformed tobacco BY-2 cells expressing our genomic GFP–KCBP construct and mRFP1–MAP4 to label microtubules (Van Damme et al., 2004). This showed that KCBP and microtubule localizations were similar but not identical during the preprophase band stage. Sites of GFP–KCBP localization were detected where microtubules appeared to be absent and some microtubules were not decorated by GFP–KCBP (Fig. 7A–D).

The same double-expressing tobacco BY-2 cell lines were then used to clarify the relationship between phragmoplast microtubules and GFP–KCBP of the CDZ. In Fig. 7E–H, a phragmoplast is shown that grows out towards the CDZ at one side of the cell. The microtubule label at the edge of the phragmoplast can be seen to connect to the CDZ, thereby bridging GFP–KCBP at the base of the phragmoplast (the distal end) with GFP–KCBP at the cortex (see arrowheads in Fig. 7H,I).

The MyTH4-FERM domain is required for localization to the cortical division plane

The kinesin KCBP from plants is unique because it possesses a calmodulin-binding domain for Ca^{2+}-mediated regulation of its C-terminal motor (Reddy et al., 1996; Narasimhulu and Reddy, 1998; Vinogradova et al., 2009) and because it has an N-terminal MyTH4-FERM domain, which is a protein–protein interaction domain found in myosin-related actin motors (Titus, 2004). Both the C-terminal and N-terminal regions of KCBP contribute to its capacity for microtubule bundling (Kao et al., 2000). To determine which part of the KCBP molecule is responsible for localization to the CDZ, a series of KCBP truncations was made, coupled to N-terminal GFP and expressed in dividing tobacco BY-2 cells (using CaMV35S-driven expression; Fig. 8A). First, we investigated whether Ca^{2+} regulation was required for KCBP localization. The first fragment, which lacked the C-terminus including the calmodulin-binding helix, located to the CDZ. Even when the entire C-terminal regulatory domain was deleted, including its neck mimic (Vinogradova et al., 2009), localization to the CDZ was observed (Fig. 8B). Therefore, as labelling of the CDZ was routinely observed with these constructs it would appear that the calmodulin-binding domain (and, by extension, Ca^{2+} regulation per se) is not required for localization of KCBP to the CDZ after preprophase band breakdown.

Next, we tested whether the motor domain of KCBP (including its Ca^{2+} responsive sequences) was sufficient for localization to the CDZ (fragment Δ8). This proved negative (Fig. 8). Testing additional fragments of KCBP showed that the MyTH4-FERM domain is involved in plasma membrane localization but that this requires the presence of its adjacent coiled coil domain (fragment Δ6) (Fig. 8C). Fragment Δ6 was found to label the cortex at preprophase, mitosis and during the phragmoplast stage. Neither the MyTH4-FERM domain nor the coiled coil region by itself conferred plasma membrane localization during cell division. One possibility is that the MyTH4-FERM domain of KCBP could require oligomerization through the neighbouring coiled coil region to facilitate CDZ localization.

Next, we modelled the structure of the KCBP MyTH4-FERM region using the available crystal structure of the MyTH4-FERM region of human Myosin X (PDB 3PZD) (Wei et al., 2011) and the Phyre2 server. Phyre2 reported a 100% confidence for the model, suggesting that the folding of the KCBP MyTH4-FERM region is

Journal of Cell Science (2015) 128, 2033-2046 doi:10.1242/jcs.156570

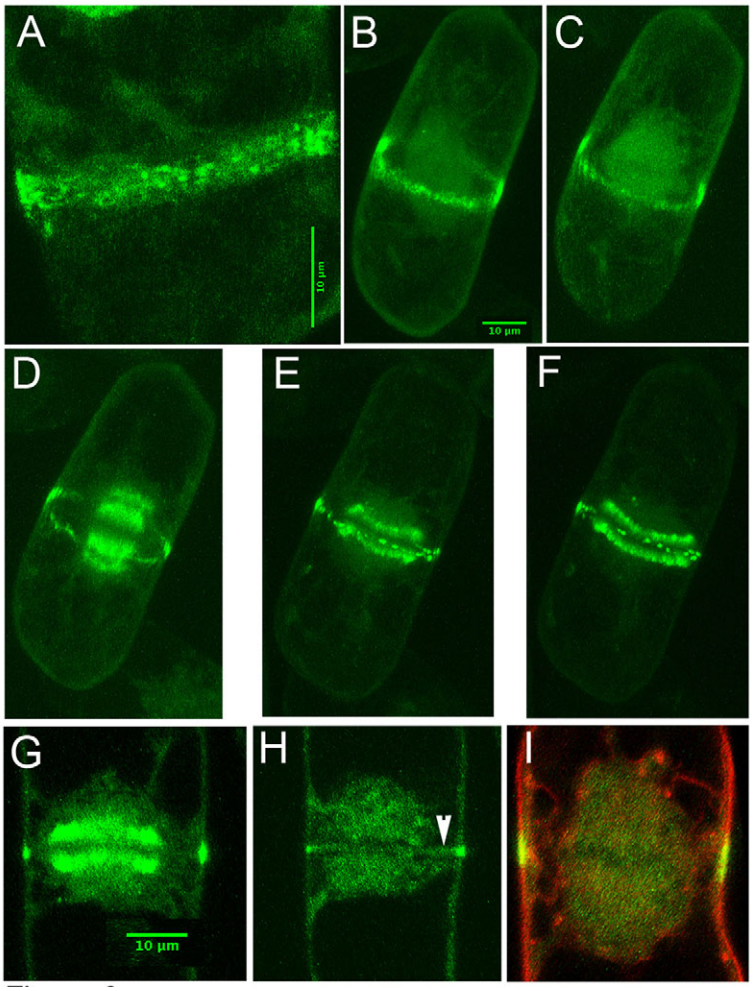

Fig. 6. Dynamics of GFP–KCBP localization during tobacco BY-2 cell division when expressed from the *KCBP* promoter. (A) During preprophase, KCBP localized to the band of microtubules. The staining was always punctate, usually showing only a few microtubule-like filaments. (B–F) A single cell was followed from pro-metaphase to cytokinesis. (B) In pro-metaphase, after nuclear envelope breakdown, KCBP remained in the cortical area previously occupied by the preprophase band. (C) In metaphase, cortical KCBP was still present in a ring encircling the cell, however, this ring now started to narrow. At this stage the spindle microtubules were not labelled by KCBP, as the spindle is hardly visible. (D,E) In ana-telophase (D) and then in telophase (E) the cortical KCBP ring became progressively narrower and the signal was finally concentrated in punctae, like beads on a string. Note that KCBP also labelled the microtubules of the anaphase and telophase spindle and of the phragmoplast, in contrast to the metaphase spindle (C). (F) In cytokinesis, the enlarging phragmoplast was seen to grow out towards the cortical KCBP punctae. (F,G) During the phragmoplast stage, it can be seen that KCBP labels only the juxta-nuclear parts of the opposing microtubule sets comprising the phragmoplast. Therefore the dark line that includes the cell plate is usually several micrometres wide. (H) After cytokinesis, KCBP showed a torus-like behaviour, with some of the label moving centripetally (arrow) into the new cross wall. (I) Colabelling experiments using the lipid dye FM4-64 (red channel) suggested that during metaphase KCBP localized directly to the plasma membrane of the cortical division site. Scale bars: 10 µm (A–I).

highly similar to that of myosin X (Fig. 8D). This high significance suggests functional similarity of the MyTH4-FERM domains of KCBP and myosin X. An alignment of 18 plant KCBPs for modelling sequence conservation in the MyTH4-FERM domain showed that the FERM-C subdomain is especially conserved among plants (Fig. 8E), underlining its importance for KCBP function.

DISCUSSION

The interaction of AIR9 with KCBP

Our previous work showed that the large microtubule-associated protein AIR9 interacts with the preprophase band of microtubules, but unlike the proteins TAN and RanGAP1 it does not remain present in the CDZ once the band has depolymerized (Buschmann et al., 2006). However, it does return as a tighter cortical ring (the CDS) just as the phragmoplast makes contact with the cortex. AIR9 then moves inwards to decorate the maturing cell plate, forming a torus. Two main findings support the idea that AIR9 directly and specifically interacts with the molecular memory of the preprophase band. First, when phragmoplasts (and cell plates) from tobacco BY-2 cells were fragmented using the herbicide CIPC, only those lobes that contacted the cortex correctly at the exact position of the CDS (i.e. those predicted by the preprophase band) produced an AIR9 torus. Cell plate insertion at aberrant positions away from the preprophase-band-predicted CDS did not produce a torus (Buschmann et al. 2006). Second, as shown in this paper (Fig. 1), when tobacco BY-2 cells expressing GFP-AIR9 were treated with brefeldin A, phragmoplasts became stalled in their expansion at early telophase; however, at the same time GFP–AIR9 could be seen to accumulate precociously at the CDZ. These results support the idea that AIR9 is capable of associating with and recognizing the preprophase memory.

We therefore hypothesized that new components of the preprophase memory could be isolated by using AIR9 as bait in a yeast two-hybrid screen against a cDNA library from *Arabidopsis* seedlings. Among other cDNAs representing putative AIR9 interactors, the screen yielded several fragments of the minus-end-directed kinesin KCBP (Reddy et al., 1996; Oppenheimer et al., 1997). The interaction of AIR9 with KCBP, as observed for the yeast nucleus, was then confirmed by immunoprecipitation from plant extracts and by pulldowns using bacterially expressed proteins (Fig. 2). When overexpressed in *Nicotiana benthamiana* epidermal leaf cells, AIR9 is capable of recruiting KCBP to the cortical microtubules, indicating a physical interaction between both proteins (Fig. 3). Furthermore, AIR9 and KCBP were shown to colocalize in the preprophase band, on cross walls and on the phragmoplast (Fig. 2). We emphasize that the localization of both proteins is not identical (e.g. only KCBP remains in the CDZ throughout mitosis and cytokinesis) and the interaction might therefore be temporary and regulated by specific signals, for instance cell cycle progression. Combined, these results support the idea that AIR9 from *Arabidopsis* interacts with a microtubule motor.

Journal of Cell Science (2015) 128, 2033-2046 doi:10.1242/jcs.156570

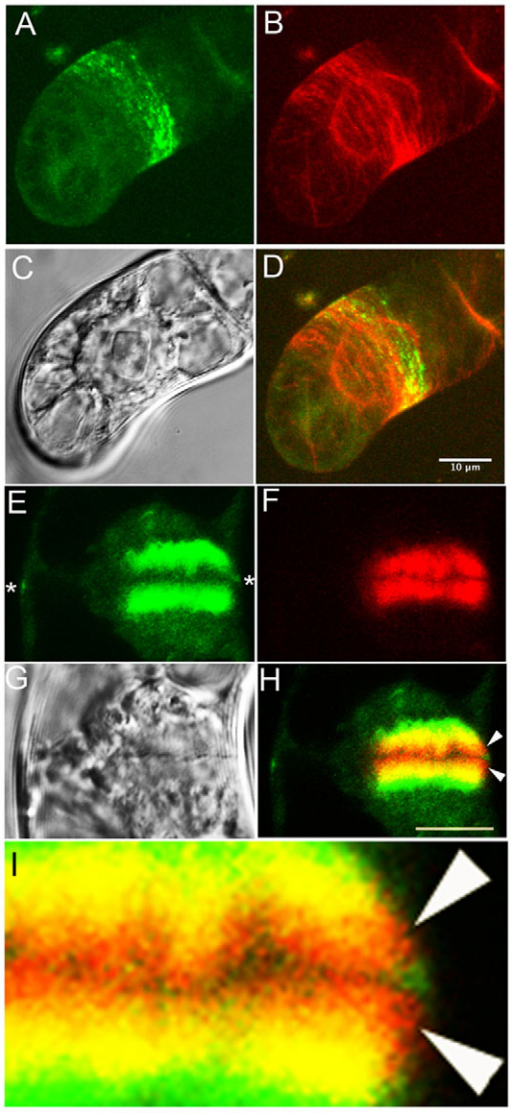

Fig. 7. GFP–KCBP localization during cell division as analysed by co-expression of the microtubule marker mRFP1–MAP4 using a confocal microscope. (A) GFP–KCBP expressed from the *KCBP* promoter labelled the preprophase band (*z*-projection). (B) The preprophase band labelled by mRFP1–MAP4 (*z*-projection). (C) The same cell in the transmission channel. (D) Merging reveals partial colocalization of KCBP with microtubules. (E) GFP–KCBP expressed from the *KCBP* promoter during cytokinesis (single confocal section). Note KCBP localization towards the phragmoplast distal end (where most microtubule minus ends are found) as well as KCBP presence in the CDZ (asterisks). (F) Phragmoplast microtubules (single section). (G) The same cell in the transmission channel. (H) Merging the channels shows that microtubules of the phragmoplast edge are directed towards KCBP at the cortical division site (arrowheads). (I) Magnification of the arriving phragmoplast seen in H. Note the microtubule label (red) connecting to KCBP (green) at the cortical division site. Scale bars: 10 µm.

GFP tagging reveals that KCBP localizes to the preprophase memory

The most notable finding of this study, however, is that GFP-tagged KCBP marks the cortical division site throughout division and as such is part of the cortical machinery that memorizes the preprophase band. Previous studies using immunofluorescence to locate KCBP have reported labelling of the preprophase band, the spindle and the phragmoplast but not the CDZ from mitosis onwards (Bowser and Reddy, 1997; Smirnova et al., 1998; Preuss et al., 2003). The absence of CDZ staining in fixation studies invites parallels with studies on TANGLED1, which only localized to the cortical division site after the introduction of live-cell GFP-tagging (Smith et al., 2001; Walker et al., 2007).

Our results show that KCBP can now be added alongside TANGLED1, RanGAP1 and the POK1 kinesin as part of the molecular machinery that 'memorizes' the narrow cortical division site to which the outgrowing phragmoplast is directed in cytokinesis (Walker et al., 2007; Xu et al., 2008; Lipka et al., 2014). In this context, it is interesting that both KCBP (this study) and TANGLED1 show remarkably similar behaviour during the transition from metaphase to cytokinesis (Fig. 6). In metaphase, both proteins form a wide band (similar to the preprophase band or CDZ), but this band then becomes narrower so that the distribution during cytokinesis resembles a fine string of beads (Walker et al., 2007; Rasmussen et al., 2011b). It will be interesting to learn how this concentrating mechanism is achieved at the molecular level.

Attempts have been made to reveal the function of KCBP in cell division by manipulating the activity of the kinesin (Vos et al., 2000; Hepler et al., 2002). The interaction of Ca^{2+}/calmodulin with KCBP interferes with microtubule binding of the motor domain (Deavours et al., 1998; Narasimhulu and Reddy, 1998), and Vos et al. (Vos et al., 2000) used microinjection of *Tradescantia* stamen hair cells to activate KCBP throughout cell division using an antibody directed against its calmodulin-binding domain. This led to the conclusion that the motor activity of KCBP is normally downregulated during metaphase but is reactivated during anaphase when its minus end activity draws microtubules together at the spindle poles. These findings are consistent with our localization results using GFP–KCBP (Figs. 5–7; supplementary material Movie 2).

The interwoven roles of F-actin and microtubules in cell division alignment

Several previous studies visualizing F-actin, and/or using actin-directed drugs, have suggested that F-actin is not only involved in phragmoplast integrity (Molchan et al., 2002; Smertenko et al., 2011) but also in phragmoplast guidance (Lloyd and Traas, 1988; Sano et al., 2005; Kojo et al., 2013). It is not, however, immediately clear how a role for actin in memorizing the division plane (as it must do in occupying the phragmosomal plane during mitosis) is compatible with the absence of F-actin from the narrow cortical ADZ (Cleary, 1995), to which the phragmoplast appears to be attracted. Defining a role for F-actin has also remained problematic because cell division appears to occur normally in several *Arabidopsis* mutants affected in the actin cytoskeleton (Nishimura et al., 2003). However, recent research has shown that myosin VIII and F-actin are required for phragmoplast guidance in the moss *Physcomitrella*. In that study, myosin VIII was not only shown to locate to the cortical division site from metaphase onwards but also to the phragmoplast midzone where it was positioned at the microtubule plus ends (Wu and Bezanilla, 2014). Future research might show whether the observations made for the protonemal cells of *Physcomitrella*, which do not contain preprophase bands, hold true for higher plants.

Concerning the relative contributions of actin and microtubules to division plane determination, it is interesting that the kinesin analysed in this study, KCBP, is a chimera of myosin with a kinesin-14 motor domain (Reddy and Day, 2000). Fig. 8 illustrates the high degree of similarity between the N-terminal MyTH4-FERM domain of KCBP and MyTH4-FERM domains found in metazoan myosin X. Sequence similarity searches suggest that KCBP is the only protein containing a MyTH4-FERM domain in *Arabidopsis*

Journal of Cell Science (2015) 128, 2033-2046 doi:10.1242/jcs.156570

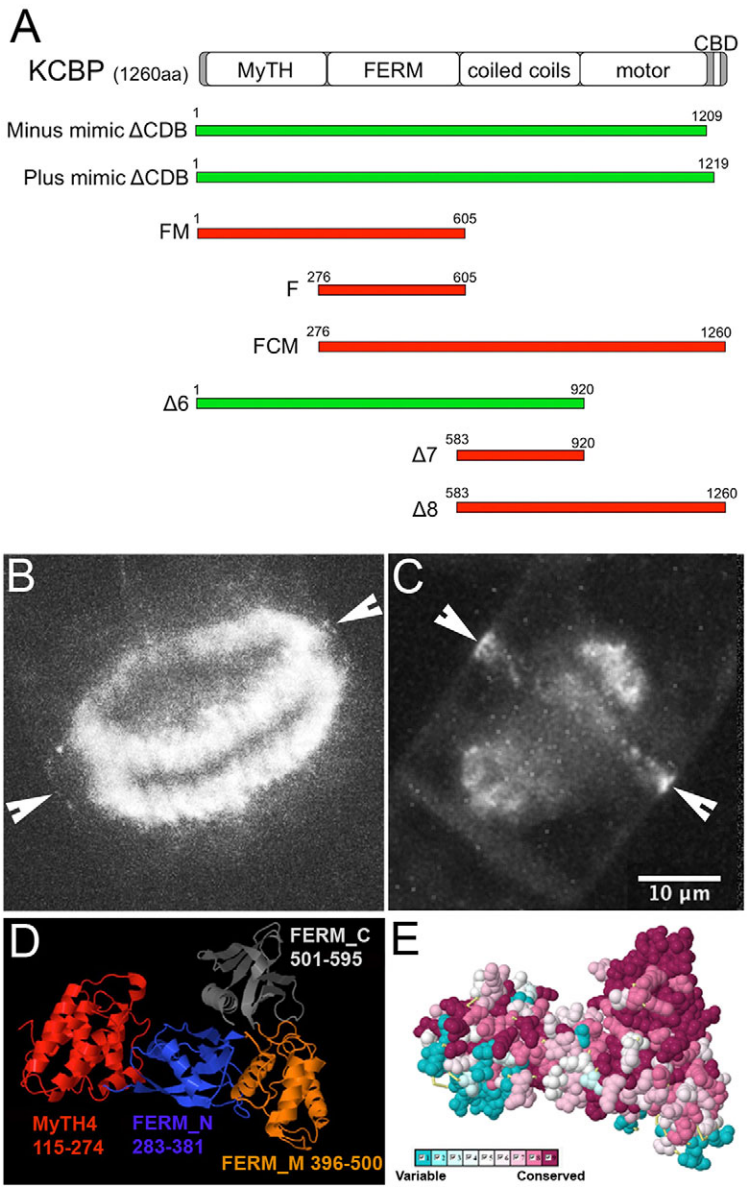

Fig. 8. KCBP truncation experiments reveal that the MyTH4-FERM domain is crucial for CDZ localization. (A) Fragments used are shown in A. Fragments with localization to the CDZ are coloured green; fragments that do not localize to the localization to the CDZ are coloured red. (B) The calmodulin-binding domain (CBD) is not required for CDZ localization during mitosis (shown here is the fragment minus mimic ΔCBD). (C) The fragment Δ6 is sufficient for CDZ localization during mitosis. (D) The MyTH4-FERM domain of KCBP (amino acids 110–620) was modelled using the solved structure from human myosin X (PDB 3PZD). (E) Conservation of the MyTH4-FERM domain of KCBP using an alignment of plant orthologs. Scale bars: 10 μm.

(data not shown) and Myosin VIII from *Physcomitrella* does not have a MyTH4-FERM domain. The MyTH4-FERM domain of myosins is required for cargo binding and several interacting proteins have been characterized, including plasma-membrane-bound receptors (Hirano et al., 2011; Wei et al., 2011; Wu et al., 2011). In this study, we show that the MyTH4-FERM domain of KCBP is involved in the localization of a kinesin-14 motor to the CDZ (Fig. 8). A similar region of KCBP is required for AIR9 interaction (Fig. 2). As AIR9 is not part of the prophase memory itself it cannot be responsible for holding KCBP in the CDZ. One possibility is that KCBP is attached through its MyTH4-FERM domain to a continuous resident of the preprophase band memory such as a membrane protein and/or a class of specialized lipids. The MyTH4-FERM domain of KCBP contains an additional microtubule-binding domain (in addition to its motor) (Narasimhulu and Reddy, 1998; Kao et al., 2000). It therefore seems possible that AIR9 is involved in regulating microtubule binding versus CDZ localization of the MyTH4-FERM domain of KCBP. Finally, it is noteworthy that some animal myosins with MyTH4-FERM domains are critically involved in cell division. Myosin X, which exhibits a MyTH4-FERM domain highly similar to KCBP (Fig. 8D), is believed to physically connect microtubules with F-actin and is required for spindle assembly and nuclear anchoring during mitosis in *Xenopus* (Weber et al., 2004).

A hypothesis for the role of KCBP in cytokinesis

What is clear is that the MyTH4-FERM domain of KCBP facilitates the localization of a minus-end-directed microtubule motor to the cortical division site, that is to the exact position where the cell plate will fuse with the plasma membrane. We have observed that so-called peripheral or exploratory microtubules that extend from the phragmoplast connect with KCBP at the cortical division site (Fig. 7H,I). Previous studies have suggested that microtubules of the phragmoplast are turned over by treadmilling and that the plus-ends of all microtubules are directed towards the cell plate (Euteneuer and McIntosh, 1980; Asada et al., 1991). However, a recent investigation demonstrated that phragmoplast microtubules show dynamic instability rather than treadmilling (Smertenko et al., 2011). Furthermore, according to this new study, nucleation of new microtubules mainly occurs on extant microtubules (thereby

Journal of Cell Science (2015) 128, 2033-2046 doi:10.1242/jcs.156570

preserving microtubule polarity), although there is also likely to be a subset of freely nucleated microtubules with opposing polarity. Because the majority of microtubules nevertheless points towards the cell plate, polar transport of cell wall material to the midline is possible (Smertenko et al., 2011). Such microtubule nucleation on the phragmoplast, together with microtubules emanating from the nuclear surfaces in late cytokinesis would explain the origin of exploratory microtubule plus ends that connect the nucleus and phragmoplast to the cortical division site (Chan et al., 2005; Dhonukshe et al., 2005). The presence of KCBP at the cortical division site therefore suggests a mechanism in which this minus-end-directed microtubule motor forms a bridgehead through which the plus ends of exploratory microtubules attach to the cortex. By processing towards the minus ends of these microtubules KCBP would effectively 'reel in' the edges of the phragmoplast. Such a model is not without precedent because cytoplasmic dynein is known to fulfil a similar function in orientating the spindles of animals and yeast. In *Saccharomyces*, dynein becomes attached to the plasma membrane where this minus-end-directed microtubule motor 'reels in' the astral microtubules and helps align the spindle poles (McNally, 2013). Similar mechanisms involving dynein and cortical pulling are at work during cell division in animals and are involved in determining the site of cytokinesis (furrowing) (Kotak and Gönczy, 2013). Flowering plants lack all types of dynein heavy chain and we hypothesize that other minus-end-directed motors, such as KCBP, have taken over some of the molecular functions performed elsewhere by this protein (Lawrence et al., 2001; Frey et al., 2010).

MATERIALS AND METHODS

Molecular cloning

An entry clone containing the *AIR9* promoter sequence was created by amplifying a 1852 base pair sequence immediately upstream of the *AIR9* translational start (this promoter sequence includes the *AIR9* 5′ UTR and its hypothetical intron) with the oligonucleotides AIR9prom_attB1and AIR9prom_attB2, and recombining the obtained DNA fragment with pDONR207. *AIR9* promoter::GUS fusions were constructed in a GATEWAY-compatible binary vector (pGWB3).

The genomic construct of KCBP labelled with N-terminal GFP was assembled using GATEWAY-compatible pGWB6. First, the CaMV35S promoter was replaced with the ~0.75 kb KCBP promoter (Reddy and Reddy, 2004) using restriction enzyme sites for *Sfb*I and *Xba*I present in pGWB6. Next, using the GATEWAY LR reaction, the entire KCBP coding region, including all introns and its 3′ UTR (contained in an entry clone derived from pDONR207), was recombined into pGWB6 carrying the KCBP promoter.

Further expression clones for CaMV35S-driven GFP-fusions (including the KCBP cDNA and its truncations) were generated using entry clones (derived from pDONR207) and destination vectors pGFP-N-BIN and pGFP-C-BIN (originally generated by Ben Trevaskis, MPI, Germany). The CaMV35S-driven mRFP1-fusions used in the experiments are derived from pH7WGR2 and pH7WRG2 destination vectors of the Ghent clone series (Karimi et al., 2002).

Oligonucleotide sequences used for the PCR-based cloning of promoters, full and partial cDNAs and genomic fragments will be quickly provided on request.

RNA *in situ* hybridization of whole tissue samples

Arabidopsis seedlings were grown on wet Whatman filter paper for 3–5 days under long day conditions. The preparation and testing of the *AIR9* antisense probe was performed as described previously (Zachgo, 2002). Fixation of the seedlings and the following whole-mount *in situ* hybridization was performed according to Hejátko et al. (Hejátko et al., 2006) but with the tissue incubation with Proteinase K (125 mg/ml) prolonged to 30 min and an additional cell wall digestion step using 1% (w/v) cellulase and 0.2% (w/v) Macerozyme (Althoff et al., 2014).

Reverse-transcriptase polymerase chain reaction

cDNAs were generated based on total RNA preparations (Qiagene) from agar-grown plants using the Superscript II Reverse Transcriptase (Invitrogene) according to the manufacturer's instructions. Oligonucleotide sequences for the amplification of *AIR9* fragments will be given on request.

AIR9 and KCBP interaction studies

Immunoprecipitations were based on protein extracts from a cycling *Arabidopsis* L*er* suspension culture (Korolev et al., 2005). Cells were harvested 3 days after sub-culturing and ground with mortar and pestle using liquid N_2. Ground cells were further homogenized in one volume immunoprecipitation buffer (50 mM Tris-HCl pH 8, 150 mM NaCl; 5 mM EDTA; 2% (v/v) Triton X-100, proteinase inhibitors by Roche) and incubated on ice for 30 min. Extracts were centrifuged (>20,000 rpm in a SS34 rotor, Sorvall) for 20 min at 4°C and the supernatant was collected. After one repeated centrifugation, the supernatant was cleared through a 0.2 µm filter. 500 µl of the supernatant were then mixed with 20 µl of a polyclonal rabbit antibody against AIR9 (Basu et al., 2005) and rotated end over end at 4°C for 1 h. Next, 50 µl of IP-buffer equilibrated protein A beads (Sigma P3476) were added to the mixture. This was further incubated under slow rotation for at least 1 h or overnight. The beads were then washed three times with cold IP buffer aided using a table-top centrifuge. Finally, the washing liquid was removed entirely before 50 µl of 2x SDS loading buffer were added to the beads. This was boiled for 5 min, cooled down and centrifuged. 15 µl of the supernatant were then subjected to SDS-PAGE using 7.5% (w/v) gels. Western blotting was performed according to standard methods, but without methanol. The blots were then probed with the rat antibody against cotton KCBP. Detection was achieved using Abcam (Cambridge, UK) secondary antibodies and a chemiluminescence kit (Thermo Scientific, Germany).

The reciprocal experiment was based on bacterially expressed proteins. The 132 kDa His-AIR9 fragment, which includes the 11 repeated A9 domains of the full-length protein, was expressed in BL21 (DE3) cells at 20°C overnight using the pET30A vector system and IPTG induction (Basu et al., 2005). The His-AIR9 fragment was purified from sonicated extracts using Nickel columns by Macherey and Nagel (Düren, Germany) according to the manufacturer's instructions. The protein was further purified and concentrated using Amicon columns (Millipore; size exclusion limit<50 kDa). GST-tagged KCBP was expressed using the pDEST15 vector and IPTG induction in BL21 DE3 cells at 20°C overnight. GST-KCBP was purified from sonicated extracts using glutathione-agarose beads (Macherey and Nagel) according to the manufacturer's instructions. The GST-KCBP protein was concentrated and purified from free glutathione using Amicon columns (size exclusion limit<50 kDa). The interaction of the 132 kDa His-AIR9 fragment with GST-KCBP was probed in PBS buffer (including protease inhibitors) at room temperature. After 50 min of gentle agitation equilibrated glutathione-agarose beads were added and the mixture was incubated for a further 30 min. The beads were then washed four times and resuspended in two-fold SDS-buffer. After polyacrylamide gel electrophoresis and western blotting His-tagged AIR9 protein was detected using antibodies by Abcam (Cambridge, UK) and a chemiluminescence kit (Thermo Scientific, Germany).

The yeast-2-hybrid screen against a cDNA library (young seedlings from *Arabidopsis*) using the 11 repeated A9 domains of AIR9 as bait was performed by the Hybrigenics company (Paris, France).

Microscopy

Fluorescent protein microscopy was performed using a spinning disc confocal by VisiTech (equipped with a Hamamatsu Orca ER detector) and various confocal microscopes from Zeiss and Leica, including Meta710-Zen and SP5 instruments, respectively. Living *Arabidopsis* seedlings and tobacco BY-2 cells (20 µl) were observed by sealing them between a coverslip and a piece of the gas-permeable Biofoil 25 membrane (VivaScience, Hannover, Germany).

In order to examine the placement of cross-walls in the *Arabidopsis* rhizodermis whole plants (7–8 days after germination) were transferred to Paul's medium containing 100 µg/ml propidium iodide and incubated in this solution for at least 30 min. Roots were observed with a confocal microscope using a x40 oil immersion objective.

Scanning electron microscopy of *Arabidopsis* leaf trichomes

Scanning electron microscopy was performed as recently described (Sambade et al., 2014). For the analysis of ovules in wild-type and hemizygous *ungud9* plants unfertilized flowers were fixed in 9:1 ethanol: acetic acid solution (v/v) for at least 30 min. Next, the specimen were transferred to pure ethanol and then to 70% (v/v) ethanol (each step 30 minutes). The flowers were then plunged into clearing solution, which consisted of 8:2:1 chloral hydrate:H_20:glycerol (w/v/v). After an overnight incubation they were examined using a x60 oil immersion objective using Nomarski optics.

Plant growth and transformation

Tobacco BY-2 cultures were cultivated as described previously (Koroleva et al., 2006) and *Arabidopsis* seedlings were grown on Paul's medium (Buschmann et al., 2011). Tobacco BY-2 cells were transformed as previously described (Korolev et al., 2005). Columbia-0 suspension cells were transiently transformed as described by Mathur et al. (Mathur et al., 1998). The transient transformation of *Nicotiana benthamiana* epidermal leaf cells through infiltration with *Agrobacterium* was performed as previously described (Niehl et al., 2012). Transformation of *Arabidopsis* was achieved by the floral dip method (Clough and Bent, 1998).

In situ β-glucuronidase (GUS) analysis

GUS staining based on *β-glucuronidase* expression (Jefferson et al., 1987) driven by the AIR9 promoter was performed as follows. Plant material was vacuum-infiltrated with fixation buffer [1% formaldehyde (w/v), 50 mM sodium phosphate buffer (pH 7), 0.05% (v/v) Triton-X-100] and incubated at room temperature for 40 min. Plant tissues were then washed three times with 50 mM sodium phosphate buffer (pH 7) and vacuum-infiltrated with GUS staining buffer [1 mM 5-bromo-4-chloro-indolyl glucuronide, 1 mM potassium hexacyanoferrate-(II), 1 mM potassium hexacyanoferrate-(III), 10 µM EDTA, 50 mM sodium phosphate buffer, 0.1% (v/v) Triton-X-100]. Samples were incubated at 37°C for 24 h. Tissues were then cleared using 70% (v/v) and 99% (v/v) ethanol washing steps. For photography, specimens were transferred to 40% (v/v) glycerol using two intermediate steps: a 70% (v/v) ethanol wash followed by an ethanol and glycerol (35% and 20%, respectively, v/v) wash. GUS-stained plants were photographed with a Nikon Eclipse 800 microscope equipped with a digital camera.

Arabidopsis mutant lines

In order to obtain strong *zwichel* mutants in Col-0 background, we ordered T-DNA insertion lines for the ZWICHEL (KCBP) gene from NASC Nottingham. The following lines were obtained: N531704 (dubbed *zwiA*) with an insertion into the third exon, N639201 (*zwiB*) with insertion into the ninth exon, N652109 (*zwiC*) with insertion into the twentieth exon. The *zwiC* insertion had only a weak trichome phenotype; however, the *zwiA* trichome phenotype was strong and comparable to *zwi9311-11* in RLD2 background (Luo and Oppenheimer, 1999). *zwiA* was used for the complementation test using the genomic GFP-KCBP fusion.

Mutants of *AIR9* were obtained from NASC, from the *Arabidopsis* TILLING project and from the laboratories of David Twell (University of Leicester, UK) and Ueli Grossniklaus (Zurich, Switzerland). See supplementary material Table S1 for details on *air9* mutants analysed in this study.

Computational protein sequence and structure analyses

The structure of the amino acid fragment 110–620 from *A. thaliana* KCBP was modelled using Phyre2 one-to-one threading (Kelley and Sternberg, 2009) with the structure of human Myosin X (chain A from PDB 3PZD) (Wei et al., 2011). A selection of 17 BLAST orthologs of *A. thaliana* KCBP was collected from the NCBI Entrez Protein database. A multiple sequence alignment of *A. thaliana* KCBP and orthologs was constructed using ClustalW (Larkin et al., 2007). The alignment and the structure models were used as an input to display residue conservation in KCBP from plants mapped on to the predicted structure using the ConSurf web tool (Ashkenazy et al., 2010).

Acknowledgements

Plasmids pGWB3 and pGWB6 were used by kind permission of Tsuyoshi Nakagawa (Department of Molecular and Functional Genomics, Shimane University, Japan). The 35S::mRFP1-MAP4 vector was kindly provided by Daniel Van Damme (VIB Department of Plant Systems Biology, Ghent University, Belgium). We are very grateful to Bo Liu (Department of Plant Biology, University of California Davis, USA) for providing the KCBP-directed antiserum and to Anireddy S.N. Reddy for advice on the cell biology of KCBP. Special thanks to Nora Gutsche for advice on handling bacterially expressed proteins. We further thank Phon Green for lab assistance and Kim Findlay and Grant Calder for help with microscopes. Seeds of *air9* deletion mutants were kindly provided by David Twell (Department of Biology, University of Leicester, United Kingdom) and Ueli Grossniklaus (Institue of Plant Biology, University of Zurich, Switzerland).

Competing interests

The authors declare no competing or financial interests.

Author contributions

H.B., J.H.D. and C.W.L. designed the research. H.B., J.D., S.K., M.A.A-N., D.B.S. and E.J.P. performed the research. H.B., M.A.A-N., S.Z., M.H. and C.W.L. analysed the data. H.B. and C.W.L. wrote the article. M.H. and J.H.D. contributed to writing.

Funding

This work was supported by the Biotechnology and Biological Sciences Research Council (BBSRC) [grant number BB/E022634/1 to C.W.L. and J.H.D.]; by an EMBO short-term fellowship [grant number ASTF 169.00-2011 to H.B.] ; and by Deutsche Forschungsgemeinschaft [grant number ZA 259/6 to S.Z.]. J.D. was supported by the Leonardo Da Vinci programme of the European Union.

Supplementary material

Supplementary material available online at
http://jcs.biologists.org/lookup/suppl/doi:10.1242/jcs.156570/-/DC1

References

Althoff, F., Kopischke, S., Zobell, O., Ide, K., Ishizaki, K., Kohchi, T. and Zachgo, S. (2014). Comparison of the MpEF1α and CaMV35 promoters for application in Marchantia polymorpha overexpression studies. *Transgenic Res.* **23**, 235-244.

Asada, T., Sonobe, S. and Shibaoka, H. (1991). Microtubule translocation in the cytokinetic apparatus of cultured tobacco cells. *Nature* **350**, 238-241.

Ashkenazy, H., Erez, E., Martz, E., Pupko, T. and Ben-Tal, N. (2010). ConSurf 2010: calculating evolutionary conservation in sequence and structure of proteins and nucleic acids. *Nucleic Acids Res.* **38**, W529-W533.

Basu, D., Le, J., El-Essal, S.-D., Huang, S., Zhang, C., Mallery, E. L., Koliantz, G., Staiger, C. J. and Szymanski, D. B. (2005). DISTORTED3/SCAR2 is a putative arabidopsis WAVE complex subunit that activates the Arp2/3 complex and is required for epidermal morphogenesis. *Plant Cell* **17**, 502-524.

Bowser, J. and Reddy, A. S. (1997). Localization of a kinesin-like calmodulin-binding protein in dividing cells of Arabidopsis and tobacco. *Plant J.* **12**, 1429-1437.

Brodersen, P., Petersen, M., Pike, H. M., Olszak, B., Skov, S., Odum, N., Jørgensen, L. B., Brown, R. E. and Mundy, J. (2002). Knockout of Arabidopsis accelerated-cell-death11 encoding a sphingosine transfer protein causes activation of programmed cell death and defense. *Genes Dev.* **16**, 490-502.

Buschmann, H., Chan, J., Sanchez-Pulido, L., Andrade-Navarro, M. A., Doonan, J. H. and Lloyd, C. W. (2006). Microtubule-associated AIR9 recognizes the cortical division site at preprophase and cell-plate insertion. *Curr. Biol.* **16**, 1938-1943.

Buschmann, H., Sanchez-Pulido, L., Andrade-Navarro, M. A. and Lloyd, C. W. (2007). Homologues of Arabidopsis microtubule-associated air9 in trypanosomatid parasites: hints on evolution and function. *Plant Signal. Behav.* **2**, 296-299.

Buschmann, H., Green, P., Sambade, A., Doonan, J. H. and Lloyd, C. W. (2011). Cytoskeletal dynamics in interphase, mitosis and cytokinesis analysed through Agrobacterium-mediated transient transformation of tobacco BY-2 cells. *New Phytol.* **190**, 258-267.

Camilleri, C., Azimzadeh, J., Pastuglia, M., Bellini, C., Grandjean, O. and Bouchez, D. (2002). The Arabidopsis TONNEAU2 gene encodes a putative novel protein phosphatase 2A regulatory subunit essential for the control of the cortical cytoskeleton. *Plant Cell* **14**, 833-845.

Chan, J., Calder, G., Fox, S. and Lloyd, C. (2005). Localization of the microtubule end binding protein EB1 reveals alternative pathways of spindle development in Arabidopsis suspension cells. *Plant Cell* **17**, 1737-1748.

Cleary, A. L. (1995). F-actin redistributions at the division site in living Tradescantia stomatal complexes as revealed by microinjection of rhodamine-phalloidin. *Protoplasma* **185**, 152-165.

Clough, S. J. and Bent, A. F. (1998). Floral dip: a simplified method for Agrobacterium-mediated transformation of Arabidopsis thaliana. *Plant J.* **16**, 735-743.
Deavours, B. E., Reddy, A. S. and Walker, R. A. (1998). Ca2+/calmodulin regulation of the Arabidopsis kinesin-like calmodulin-binding protein. *Cell Motil. Cytoskeleton* **40**, 408-416.
Dhonukshe, P., Mathur, J., Hülskamp, M. and Gadella, T. W.Jr (2005). Microtubule plus-ends reveal essential links between intracellular polarization and localized modulation of endocytosis during division-plane establishment in plant cells. *BMC Biol.* **3**, 11.
Dixit, R. and Cyr, R. (2002). Golgi secretion is not required for marking the preprophase band site in cultured tobacco cells. *Plant J.* **29**, 99-108.
Euteneuer, U. and McIntosh, J. R. (1980). Polarity of midbody and phragmoplast microtubules. *J. Cell Biol.* **87**, 509-515.
Frey, N., Klotz, J. and Nick, P. (2010). A kinesin with calponin-homology domain is involved in premitotic nuclear migration. *J. Exp. Bot.* **61**, 3423-3437.
Gunning, B. E. and Wick, S. M. (1985). Preprophase bands, phragmoplasts, and spatial control of cytokinesis. *J. Cell Sci.* 1985 Suppl. **2**, 157-179.
Hejátko, J., Blilou, I., Brewer, P. B., Friml, J., Scheres, B. and Benková, E. (2006). In situ hybridization technique for mRNA detection in whole mount Arabidopsis samples. *Nat. Protoc.* **1**, 1939-1946.
Hepler, P. K., Valster, A., Molchan, T. and Vos, J. W. (2002). Roles for kinesin and myosin during cytokinesis. *Philos. Trans. R. Soc. B* **357**, 761-766.
Hirano, Y., Hatano, T., Takahashi, A., Toriyama, M., Inagaki, N. and Hakoshima, T. (2011). Structural basis of cargo recognition by the myosin-X MyTH4-FERM domain. *EMBO J.* **30**, 2734-2747.
Hülskamp, M., Misŕa, S. and Jürgens, G. (1994). Genetic dissection of trichome cell development in Arabidopsis. *Cell* **76**, 555-566.
Jefferson, R. A., Kavanagh, T. A. and Bevan, M. W. (1987). GUS fusions: beta-glucuronidase as a sensitive and versatile gene fusion marker in higher plants. *EMBO J.* **6**, 3901-3907.
Jürgens, G. (2005). Cytokinesis in higher plants. *Annu. Rev. Plant Biol.* **56**, 281-299.
Kao, Y. L., Deavours, B. E., Phelps, K. K., Walker, R. A. and Reddy, A. S. (2000). Bundling of microtubules by motor and tail domains of a kinesin-like calmodulin-binding protein from Arabidopsis: regulation by Ca(2+)/Calmodulin. *Biochem. Biophys. Res. Commun.* **267**, 201-207.
Karahara, I., Suda, J., Tahara, H., Yokota, E., Shimmen, T., Misaki, K., Yonemura, S., Staehelin, L. A. and Mineyuki, Y. (2009). The preprophase band is a localized center of clathrin-mediated endocytosis in late prophase cells of the onion cotyledon epidermis. *Plant J.* **57**, 819-831.
Karimi, M., Inzé, D. and Depicker, A. (2002). GATEWAY vectors for Agrobacterium-mediated plant transformation. *Trends Plant Sci.* **7**, 193-195.
Kelley, L. A. and Sternberg, M. J. (2009). Protein structure prediction on the Web: a case study using the Phyre server. *Nat. Protoc.* **4**, 363-371.
Kojo, K. H., Higaki, T., Kutsuna, N., Yoshida, Y., Yasuhara, H. and Hasezawa, S. (2013). Roles of cortical actin microfilament patterning in division plane orientation in plants. *Plant Cell Physiol.* **54**, 1491-1503.
Korolev, A. V., Chan, J., Naldrett, M. J., Doonan, J. H. and Lloyd, C. W. (2005). Identification of a novel family of 70 kDa microtubule-associated proteins in Arabidopsis cells. *Plant J.* **42**, 547-555.
Koroleva, O. A., Roberts, G. R., Tomlinson, M. L. and Doonan, J. H. (2006). Novel approaches for cell cycle analysis in BY-2. In *Tobacco BY-2 Cells: From Cellular Dynamics to Omics* (ed. T. Nagata, K. Matsuoka and D. Inze), pp. 3-21. Berlin; Heidelberg; New York: Springer.
Kotak, S. and Gönczy, P. (2013). Mechanisms of spindle positioning: cortical force generators in the limelight. *Curr. Opin. Cell Biol.* **25**, 741-748.
Lalanne, E., Michaelidis, C., Moore, J. M., Gagliano, W., Johnson, A., Patel, R., Howden, R., Vielle-Calzada, J. P., Grossniklaus, U. and Twell, D. (2004). Analysis of transposon insertion mutants highlights the diversity of mechanisms underlying male progamic development in Arabidopsis. *Genetics* **167**, 1975-1986.
Larkin, M. A., Blackshields, G., Brown, N. P., Chenna, R., McGettigan, P. A., McWilliam, H., Valentin, F., Wallace, I. M., Wilm, A., Lopez, R. et al. (2007). Clustal W and Clustal X version 2.0. *Bioinformatics* **23**, 2947-2948.
Lawrence, C. J., Morris, N. R., Meagher, R. B. and Dawe, R. K. (2001). Dyneins have run their course in plant lineage. *Traffic* **2**, 362-363.
Lipka, E. and Müller, S. (2012). Potential roles for Kinesins at the cortical division site. *Front. Plant Sci.* **3**, 158.
Lipka, E., Gadeyne, A., Stockle, D., Zimmermann, S., De Jaeger, G., Ehrhardt, D.W., Kirik, V., Van Damme, D., and Muller, S. (2014). The phragmoplast-orienting kinesin-12 class proteins translate the positional information of the preprophase band to establish the cortical division zone in Arabidopsis thaliana. *Plant Cell* **26**, 2617-2632.
Lloyd, C. W. and Traas, J. A. (1988). The role of F-actin in determining the division plane of carrot suspension cells – drug studies. *Development* **102**, 211-221.
Luo, D. and Oppenheimer, D. G. (1999). Genetic control of trichome branch number in Arabidopsis: the roles of the FURCA loci. *Development* **126**, 5547-5557.
Mathur, J., Szabados, L., Schaefer, S., Grunenberg, B., Lossow, A., Jonas-Straube, E., Schell, J., Koncz, C. and Koncz-Kálmán, Z. (1998). Gene identification with sequenced T-DNA tags generated by transformation of Arabidopsis cell suspension. *Plant J.* **13**, 707-716.
May, S. F., Peacock, L., Almeida Costa, C. I., Gibson, W. C., Tetley, L., Robinson, D. R. and Hammarton, T. C. (2012). The Trypanosoma brucei AIR9-like protein is cytoskeleton-associated and is required for nucleus positioning and accurate cleavage furrow placement. *Mol. Microbiol.* **84**, 77-92.
McNally, F. J. (2013). Mechanisms of spindle positioning. *J. Cell Biol.* **200**, 131-140.
Mineyuki, Y. (1999). The preprophase band of microtubules: its function as a cytokinetic apparatus in higher plants. *Int. Rev. Cytol.* **187**, 1-49.
Mineyuki, Y., Marc, J. and Palevitz, B. A. (1989). Development of the preprophase band from random cytoplasmic microtubules in guard mother cells of Allium cepa L. *Planta* **178**, 291-296.
Molchan, T. M., Valster, A. H. and Hepler, P. K. (2002). Actomyosin promotes cell plate alignment and late lateral expansion in Tradescantia stamen hair cells. *Planta* **214**, 683-693.
Müller, S. (2012). Universal rules for division plane selection in plants. *Protoplasma* **249**, 239-253.
Müller, S., Han, S. and Smith, L. G. (2006). Two kinesins are involved in the spatial control of cytokinesis in Arabidopsis thaliana. *Curr. Biol.* **16**, 888-894.
Narasimhulu, S. B. and Reddy, A. S. (1998). Characterization of microtubule binding domains in the Arabidopsis kinesin-like calmodulin binding protein. *Plant Cell* **10**, 957-965.
Nebenführ, A., Frohlick, J. A. and Staehelin, L. A. (2000). Redistribution of Golgi stacks and other organelles during mitosis and cytokinesis in plant cells. *Plant Physiol.* **124**, 135-152.
Niehl, A., Amari, K., Gereige, D., Brandner, K., Mély, Y. and Heinlein, M. (2012). Control of Tobacco mosaic virus movement protein fate by CELL-DIVISION-CYCLE protein48. *Plant Physiol.* **160**, 2093-2108.
Nishimura, T., Yokota, E., Wada, T., Shimmen, T. and Okada, K. (2003). An Arabidopsis ACT2 dominant-negative mutation, which disturbs F-actin polymerization, reveals its distinctive function in root development. *Plant Cell Physiol.* **44**, 1131-1140.
Oppenheimer, D. G., Pollock, M. A., Vacik, J., Szymanski, D. B., Ericson, B., Feldmann, K. and Marks, M. D. (1997). Essential role of a kinesin-like protein in Arabidopsis trichome morphogenesis. *Proc. Natl. Acad. Sci. USA* **94**, 6261-6266.
Page, D. R., Köhler, C., Da Costa-Nunes, J. A., Baroux, C., Moore, J. M. and Grossniklaus, U. (2004). Intrachromosomal excision of a hybrid Ds element induces large genomic deletions in Arabidopsis. *Proc. Natl. Acad. Sci. USA* **101**, 2969-2974.
Pickett-Heaps, J. D. and Northcote, D. H. (1966). Organization of microtubules and endoplasmic reticulum during mitosis and cytokinesis in wheat meristems. *J. Cell Sci.* **1**, 109-120.
Preuss, M. L., Delmer, D. P. and Liu, B. (2003). The cotton kinesin-like calmodulin-binding protein associates with cortical microtubules in cotton fibers. *Plant Physiol.* **132**, 154-160.
Rasmussen, C. G., Humphries, J. A. and Smith, L. G. (2011a). Determination of symmetric and asymmetric division planes in plant cells. *Annu. Rev. Plant Biol.* **62**, 387-409.
Rasmussen, C. G., Sun, B. and Smith, L. G. (2011b). Tangled localization at the cortical division site of plant cells occurs by several mechanisms. *J. Cell Sci.* **124**, 270-279.
Reddy, A. S. and Day, I. S. (2000). The role of the cytoskeleton and a molecular motor in trichome morphogenesis. *Trends Plant Sci.* **5**, 503-505.
Reddy, V. S. and Reddy, A. S. (2004). Developmental and cell-specific expression of ZWICHEL is regulated by the intron and exon sequences of its gene. *Plant Mol. Biol.* **54**, 273-293.
Reddy, A. S., Safadi, F., Narasimhulu, S. B., Golovkin, M. and Hu, X. (1996). A novel plant calmodulin-binding protein with a kinesin heavy chain motor domain. *J. Biol. Chem.* **271**, 7052-7060.
Reichardt, I., Stierhof, Y. D., Mayer, U., Richter, S., Schwarz, H., Schumacher, K. and Jürgens, G. (2007). Plant cytokinesis requires de novo secretory trafficking but not endocytosis. *Curr. Biol.* **17**, 2047-2053.
Richardson, D. N., Simmons, M. P. and Reddy, A. S. (2006). Comprehensive comparative analysis of kinesins in photosynthetic eukaryotes. *BMC Genomics* **7**, 18.
Sambade, A., Findlay, K., Schäffner, A. R., Lloyd, C. W. and Buschmann, H. (2014). Actin-dependent and -independent functions of cortical microtubules in the differentiation of Arabidopsis leaf trichomes. *Plant Cell* **26**, 1629-1644.
Sano, T., Higaki, T., Oda, Y., Hayashi, T. and Hasezawa, S. (2005). Appearance of actin microfilament 'twin peaks' in mitosis and their function in cell plate formation, as visualized in tobacco BY-2 cells expressing GFP-fimbrin. *Plant J.* **44**, 595-605.
Smertenko, A. P., Piette, B. and Hussey, P. J. (2011). The origin of phragmoplast asymmetry. *Curr. Biol.* **21**, 1924-1930.
Smirnova, E. A., Reddy, A. S., Bowser, J. and Bajer, A. S. (1998). Minus end-directed kinesin-like motor protein, Kcbp, localizes to anaphase spindle poles in Haemanthus endosperm. *Cell Motil. Cytoskeleton* **41**, 271-280.
Smith, L. G., Gerttula, S. M., Han, S. and Levy, J. (2001). Tangled1: a microtubule binding protein required for the spatial control of cytokinesis in maize. *J. Cell Biol.* **152**, 231-236.

Song, H., Golovkin, M., Reddy, A. S. and Endow, S. A. (1997). In vitro motility of AtKCBP, a calmodulin-binding kinesin protein of Arabidopsis. *Proc. Natl. Acad. Sci. USA* **94**, 322-327.
Spinner, L., Gadeyne, A., Belcram, K., Goussot, M., Moison, M., Duroc, Y., Eeckhout, D., De Winne, N., Schaefer, E., Van De Slijke, E. et al. (2013). A protein phosphatase 2A complex spatially controls plant cell division. *Nat. Commun.* **4**, 1863.
Sundaresan, V., Springer, P., Volpe, T., Haward, S., Jones, J. D., Dean, C., Ma, H. and Martienssen, R. (1995). Patterns of gene action in plant development revealed by enhancer trap and gene trap transposable elements. *Genes Dev.* **9**, 1797-1810.
Titus, M. A. (2004). Cell biology: myosins meet microtubules. *Nature* **431**, 252-253.
Torres-Ruiz, R. A. and Jürgens, G. (1994). Mutations in the FASS gene uncouple pattern formation and morphogenesis in Arabidopsis development. *Development* **120**, 2967-2978.
Traas, J. A., Doonan, J. H., Rawlins, D. J., Shaw, P. J., Watts, J. and Lloyd, C. W. (1987). An actin network is present in the cytoplasm throughout the cell cycle of carrot cells and associates with the dividing nucleus. *J. Cell Biol.* **105**, 387-395.
Van Damme, D., Bouget, F. Y., Van Poucke, K., Inzé, D. and Geelen, D. (2004). Molecular dissection of plant cytokinesis and phragmoplast structure: a survey of GFP-tagged proteins. *Plant J.* **40**, 386-398.
Van Damme, D., Coutuer, S., De Rycke, R., Bouget, F. Y., Inzé, D. and Geelen, D. (2006). Somatic cytokinesis and pollen maturation in Arabidopsis depend on TPLATE, which has domains similar to coat proteins. *Plant Cell* **18**, 3502-3518.
Van Damme, D., Vanstraelen, M. and Geelen, D. (2007). Cortical division zone establishment in plant cells. *Trends Plant Sci.* **12**, 458-464.
Van Damme, D., Gadeyne, A., Vanstraelen, M., Inzé, D., Van Montagu, M. C., De Jaeger, G., Russinova, E. and Geelen, D. (2011). Adaptin-like protein TPLATE and clathrin recruitment during plant somatic cytokinesis occurs via two distinct pathways. *Proc. Natl. Acad. Sci. USA* **108**, 615-620.
Vanstraelen, M., Van Damme, D., De Rycke, R., Mylle, E., Inzé, D. and Geelen, D. (2006). Cell cycle-dependent targeting of a kinesin at the plasma membrane demarcates the division site in plant cells. *Curr. Biol.* **16**, 308-314.
Vinogradova, M. V., Malanina, G. G., Reddy, A. S. and Fletterick, R. J. (2009). Structure of the complex of a mitotic kinesin with its calcium binding regulator. *Proc. Natl. Acad. Sci. USA* **106**, 8175-8179.
Vos, J. W., Safadi, F., Reddy, A. S. and Hepler, P. K. (2000). The kinesin-like calmodulin binding protein is differentially involved in cell division. *Plant Cell* **12**, 979-990.
Walker, K. L., Müller, S., Moss, D., Ehrhardt, D. W. and Smith, L. G. (2007). Arabidopsis TANGLED identifies the division plane throughout mitosis and cytokinesis. *Curr. Biol.* **17**, 1827-1836.
Weber, K. L., Sokac, A. M., Berg, J. S., Cheney, R. E. and Bement, W. M. (2004). A microtubule-binding myosin required for nuclear anchoring and spindle assembly. *Nature* **431**, 325-329.
Wei, Z., Yan, J., Lu, Q., Pan, L. and Zhang, M. (2011). Cargo recognition mechanism of myosin X revealed by the structure of its tail MyTH4-FERM tandem in complex with the DCC P3 domain. *Proc. Natl. Acad. Sci. USA* **108**, 3572-3577.
Wright, A. J., Gallagher, K. and Smith, L. G. (2009). discordia1 and alternative discordia1 function redundantly at the cortical division site to promote preprophase band formation and orient division planes in maize. *Plant Cell* **21**, 234-247.
Wu, S. Z. and Bezanilla, M. (2014). Myosin VIII associates with microtubule ends and together with actin plays a role in guiding plant cell division. *eLife* **3**, 3.
Wu, L., Pan, L., Wei, Z. and Zhang, M. (2011). Structure of MyTH4-FERM domains in myosin VIIa tail bound to cargo. *Science* **331**, 757-760.
Xu, X. M., Zhao, Q., Rodrigo-Peiris, T., Brkljacic, J., He, C. S., Müller, S. and Meier, I. (2008). RanGAP1 is a continuous marker of the Arabidopsis cell division plane. *Proc. Natl. Acad. Sci. USA* **105**, 18637-18642.
Zachgo, S. (2002). In situ hybridization. In *Molecular Plant Biology: A Practical Approach*, Vol. 2 (ed. P. Gillmartin and C. Bowler), pp. 41-63. Oxford: IRL Press.

***Arabidopsis* KCBP interacts with AIR9 but stays in the cortical division zone throughout mitosis via its MyTH4-FERM domain**

Buschmann et al.

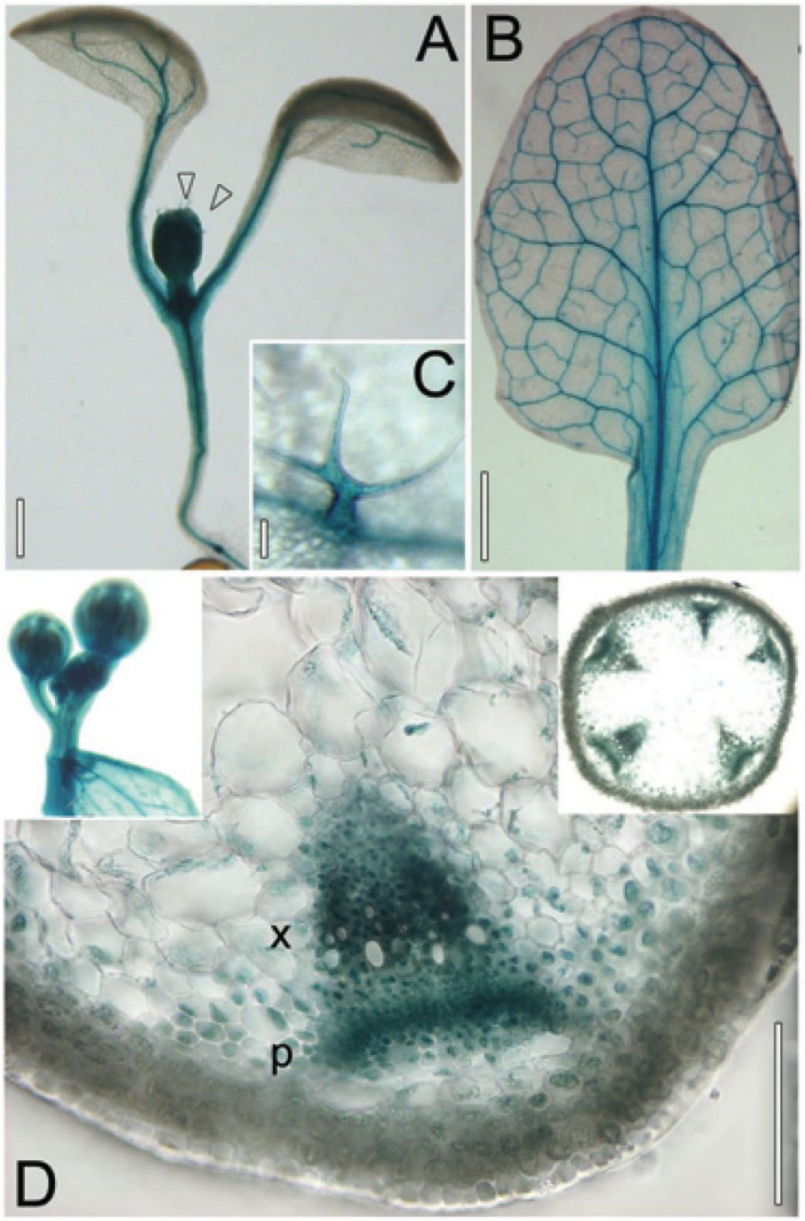

Suppl. Figure 1. Patterns of GUS expression as directed by the 1852 bp *AIR9* promoter. (A) A six-day-old *Arabidopsis* seedling has strongest expression in the vasculature, but expression is also seen in epidermal and cortical cells of hypocotyls and petioles;

arrowheads show expression in expanding leaves. (B) *AIR9* is expressed in the vasculature of rosette leaves. (C) Expression in *Arabidopsis* leaf trichomes. (D) The *AIR9* promoter directs expression to the inflorescence. Strong expression is seen in the vascular bundles; X xylem, P phloem. Stem sections varied in intensity; a section of medium intensity is displayed. Right inset shows an overview of the total stem section, left inset shows the inflorescence tip. Bars (A, B) 1 mm; (C, D) 100 µm.

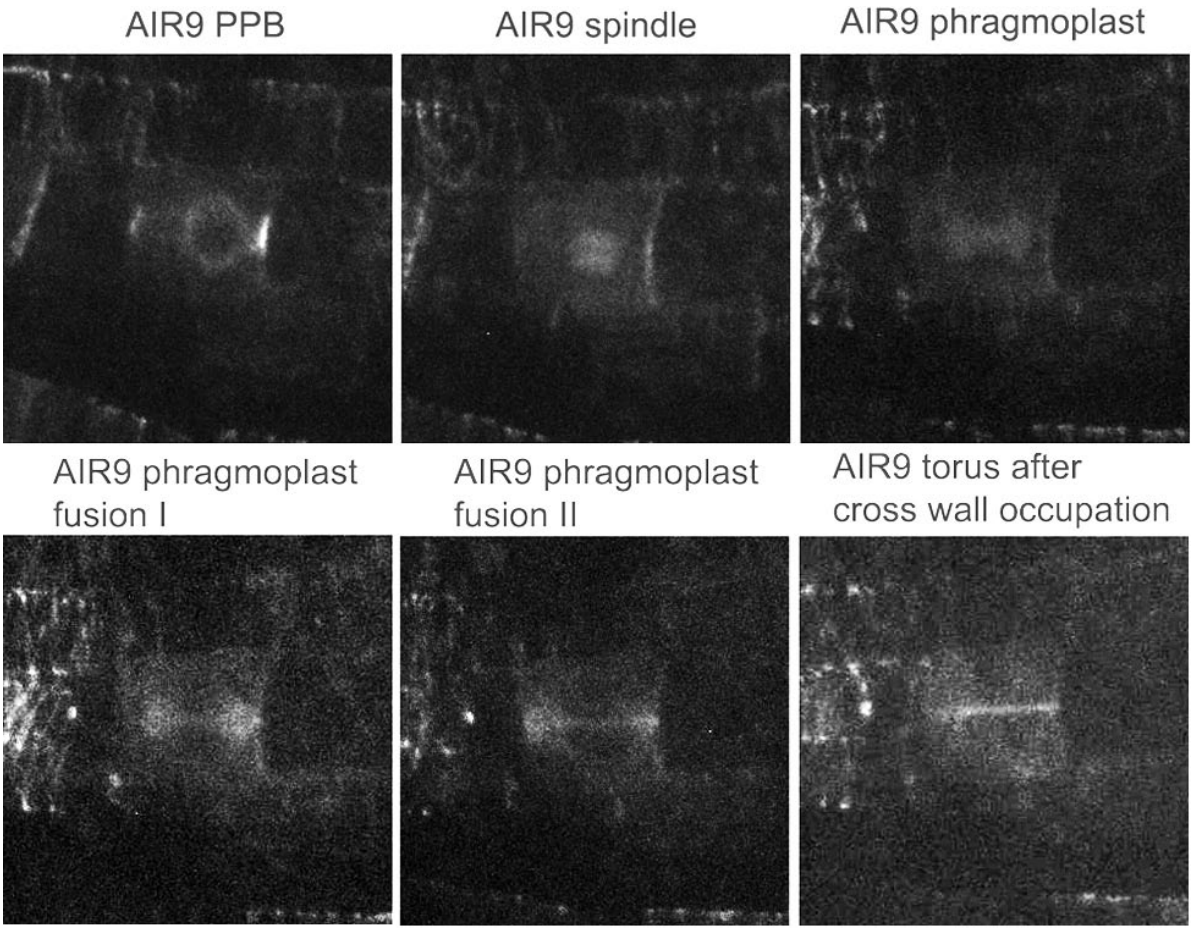

Suppl. Figure 2. GFP-AIR9 localization in the cell division of *Arabidopsis* root meristems. The fusion protein is driven by the CaMV35S promoter. GFP-AIR9 labels the the preprophase band. Note cortical GFP-AIR9 signal at cell plate insertion (best seen at "phragmoplast fusion 1").

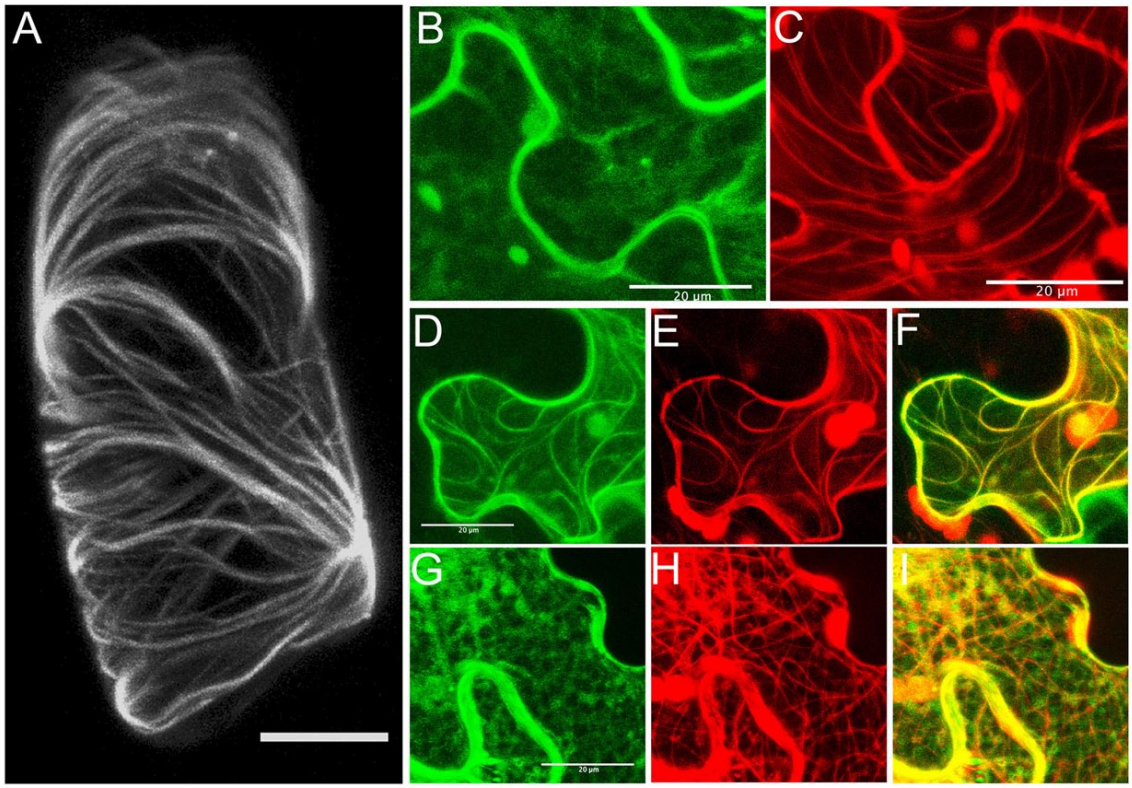

Suppl. Figure 3. Overexpression of AIR9 can lead to microtubule bundling and experiments showing that KCBP localization depends on AIR9 expression. (A) *Arabidopsis* Col-0 suspension cells were transiently transformed with 35S::GFP-AIR9. Note bundled cortical microtubules. (B) to (I) Localization patterns obtained by transiently expressing C-terminally labelled KCBP in *Nicotina benthamiana* using *Agrobacterium*. (B) KCBP-GFP expression alone hardly showed any filaments. The label was mainly cytoplasmic and somewhat reticulate. (C) mRFP1-AIR9 expression led to microtubule bundling. (D) to (F) When KCBP-GFP and mRFP1-AIR9 were co-expressed, KCBP was re-distributed to microtubules. KCBP and AIR9 localization was therefore nearly identical. (G) to (I) Co-expression of KCBP-GFP with mRFP1-MAP4 does not have an obvious effect on KCBP localization. Bars (A) 10 µm and (B) to (I) 20 µm.

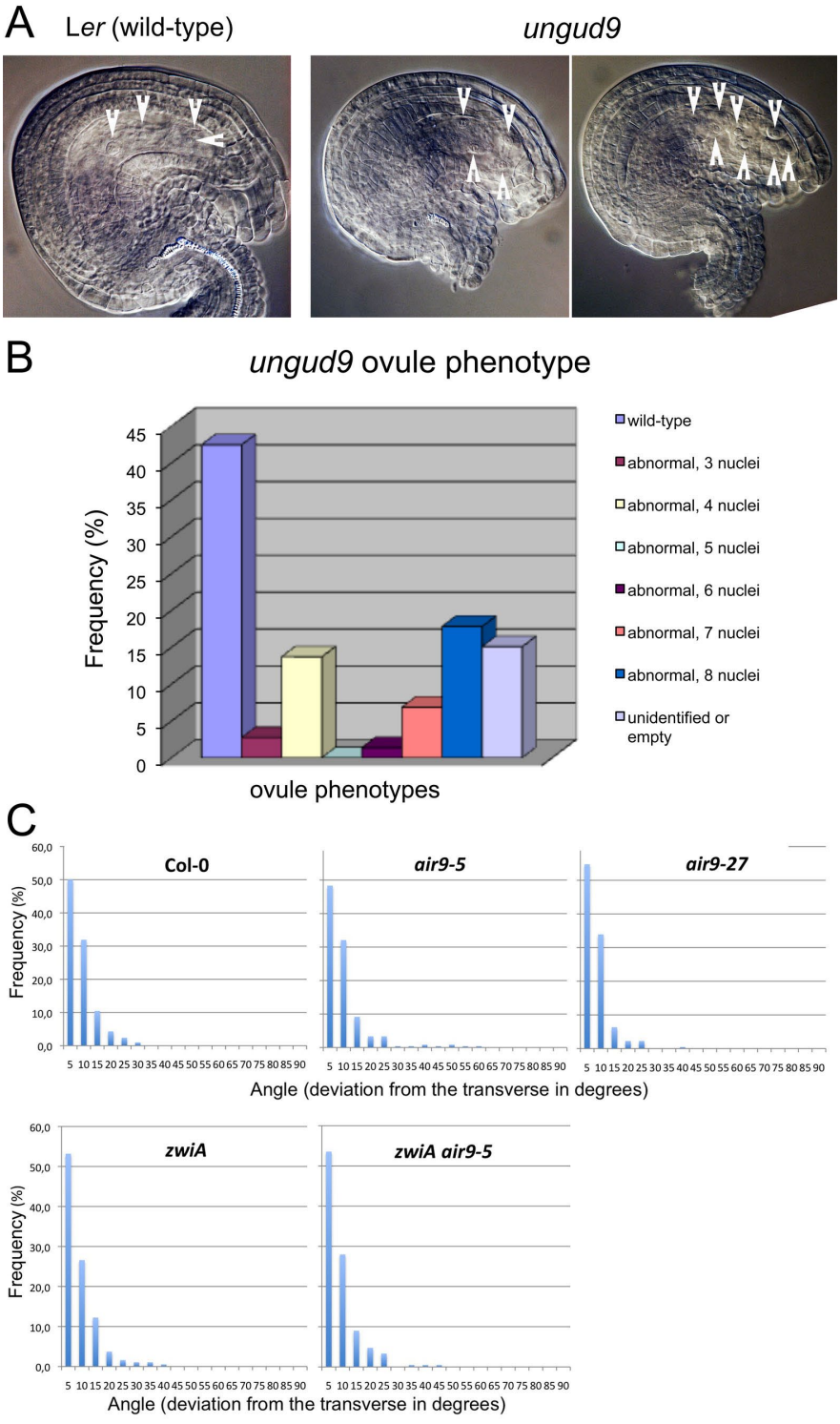

Suppl. Figure 4. Phenotypes produced by mutations involving *AIR9* and *ZWICHEL* genes. (A, B) Cell division and ovule differentiation defects in *ungud9* mutants as

compared to wild-type. *ungud9* mutants carry a large mutation involving *AIR9* and genes in its vicinity. Flowers of hemizygous *ungud9* plants produce a large proportion of abnormal ovules. (A) Micrographs of wild-type and typical *ungud9* ovules. Arrowheads point to nuclei. The wild-type image is an assembled image to show all nuclei present. In contrast, the *ungud9* images are each made of only one focus layer. These showed all nuclei present. (B) Quantification of ovule phenotypes. Note that the four and eight nuclei phenotypes were most frequent. (C) Quantification of rhizodermal cell division patterns in wild-type, *air9*, *zwi* and *air9 zwi* double mutants. Plants were grown for 7d on solid Paul's medium and subsequently stained with propidium iodide. Cross wall orientation was scored in relation to the long axis of the root (zero degrees is transverse). Measurements were done in the differentiation zone before root hair emergence. Each histogram is based on at least nine roots and at least 188 cross walls per genotype.

Suppl. Movie 1. GFP-AIR9 localization in tobacco BY-2 observed with a spinning disc confocal microscope. The movie is an assembly of projected Z-stacks acquired every 2 minutes, played back with 14 frames per second.

Suppl. Movie 2. KCBP tagged with C-terminal GFP is a continuous resident of the CDZ. The movie is an assembly of projected Z-stacks acquired every 2 minutes, played back with 10 frames per second. Note that cell shows some movement in z-direction.

Suppl. Table 1. Selected mutants of the *AIR9* gene.

Movie 1.

Movie 2.

Table S1. Selected Mutants of the *AIR9* gene.

Mutant	Synonym	Ecotype	Origin	Miscellaneous	Oligonucleotides for detection	Genotype analyzed	Sporophytic (morphological) phenotype	Gametophytic (morphological) phenotype
air9-3	N613677	Col-0	Salk T-DNA	-	LBb1 (AIR9_3034R) + AIR9_1817F	homozygous	None observed	None observed
air9-4	N175844	Ler	EXOTIC transposon	GUS inverted with respect to *AIR9* promoter	GUS2R (AIR9_2494F) + AIR9_3034R	homozygous	None observed, GUS expression present	None observed
air9-5	N517411	Col-0	Salk T-DNA	-	LBb1 (AIR9_3338F) + AIR9_3595R	homozygous	None observed	None observed
air9-9	*ungud9*	Ler	Cold Spring Harbour transposon	Carries an 11 gene deletion including part of *AIR9*. Does not breed homozygous	SGT_DS3-1 (AIR9_2230F) + AIR9gnm7511R	heterozygous	None observed	Ovule differentiation and pollen germination defect
air9-13	N93825	Col-er	TILLING	Exon/intron junction (HindIII dCAPs)	AIR9gnm_HIII_7789R + AIR9gnm_AflII_7593F	homozygous	Some phenotypes segregating, but linkage was not observed	None observed
air9-20	N172847	Ler	EXOTIC transposon	GUS correctly oriented towards *AIR9* promoter	GUS2R (AIR9_gnm5200R) + AIR9_1962F	homozygous	None observed, GUS expression present	None observed
air9-27	N902979	Col-2	WiscDsLox T-DNA	Insertion in 1. Exon at 120 bp after ATG	L4 (AIR9_420R) + AIR9_min681F	homozygous	None observed	None observed
air9-29	DSG-1	Ler	Cold Spring Harbour T-DNA	The T-DNA carries an DS element; used as transposition starter line	SGT_DS3-1 (AIR9_2230F) + AIR9gnm7511R	homozygous	None observed	None observed
air9-30	*haumea*	Ler	Cold Spring Harbour transposon	Carries a large deletion including part of *AIR9*	-	-	-	Ovule differentiation and pollen germination defect
air9-31	GT3730	Ler	Cold Spring Harbour transposon	Transposon inversion, deletion of 5' *AIR9* sequences	SGT_DS5_1 (AIR9_2230F) + AIR9 gnm7511R	homozygous	None observed	None observed